INFLUENCE OF MIXED ANIONIC-NONIONIC SURFACTANTS ON METHANE HYDRATE FORMATION: SUPPRESSION OF FOAM FORMATION

Chakorn Viriyakul

A Thesis Submitted in Partial Fulfillment of the Requirements
for the Degree of Master of Science
The Petroleum and Petrochemical College, Chulalongkorn University
in Academic Partnership with
The University of Michigan, The University of Oklahoma,
Case Western Reserve University, and Institut Français du Pétrole
2020

Influence of Mixed Anionic-Nonionic Surfactants on Methane
Hydrate Formation: Suppression of Foam Formation

Mr. Chakorn Viriyakul

A Thesis Submitted in Partial Fulfillment of the Requirements
for the Degree of Master of Science in Petrochemical Technology
Common Course
the Petroleum and Petrochemical College
Chulalongkorn University
Academic Year 2019
Copyright of Chulalongkorn University

ผลของสารลดแรงตึงผิวต่อการลดการเกิดโฟมเพื่อใช้กับการกักเก็บแก๊สธรรมชาติด้วยไฮเดรต

นายชากรณ์ วิริยะกุล

วิทยานิพนธ์นี้เป็นส่วนหนึ่งของการศึกษาตามหลักสูตรปริญญาวิทยาศาสตรมหาบัณฑิต
สาขาวิชาเทคโนโลยีปิโตรเคมี ไม่สังกัดภาควิชา/...
วิทยาลัยปิโตรเลียมและปิโตรเคมี จุฬาลงกรณ์มหาวิทยาลัย
ปีการศึกษา 2562

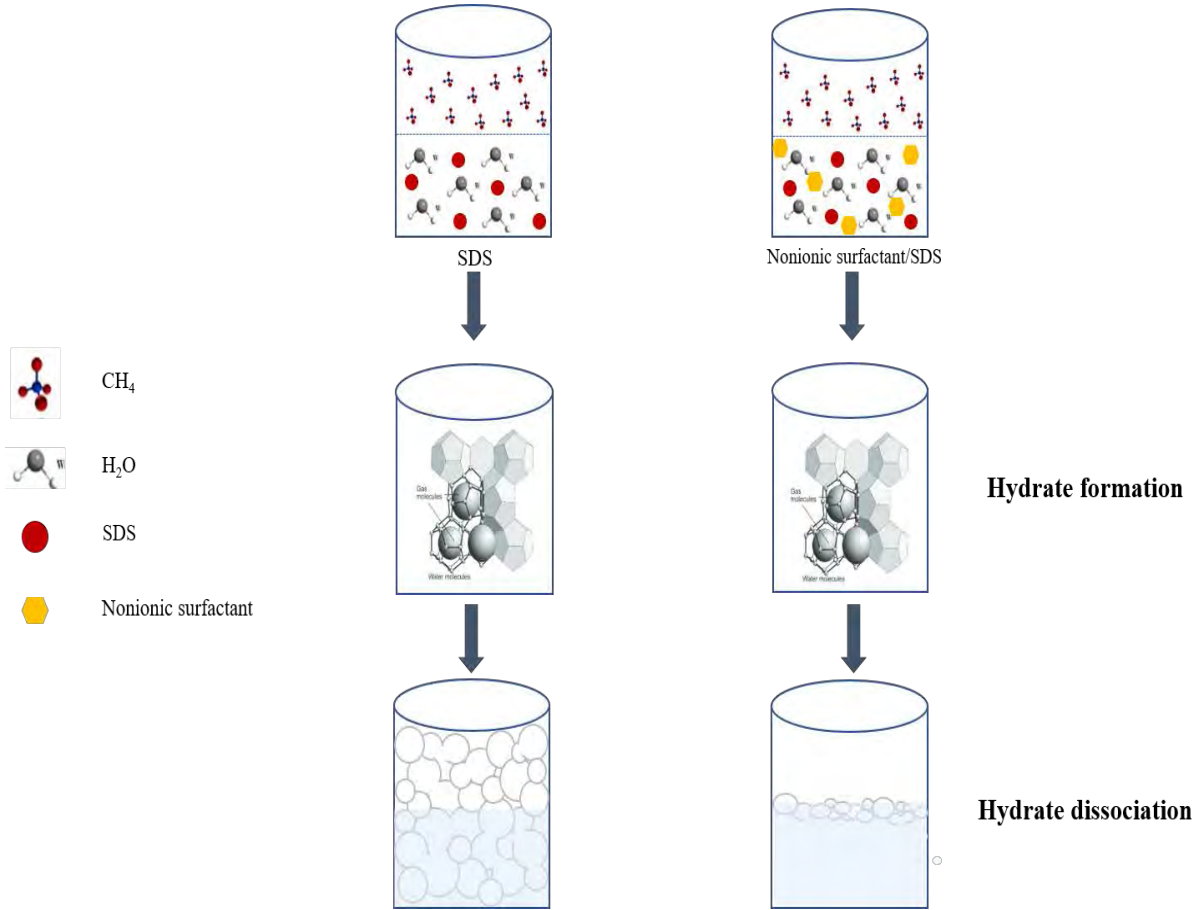|	
Thesis Title	Influence of Mixed Anionic-Nonionic Surfactants on Methane Hydrate Formation: Suppression of Foam Formation
By	Mr. Chakorn Viriyakul
Field of Study	Petrochemical Technology
Thesis Advisor	Professor PRAMOCH RANGSUNVIGIT, Ph.D.
Thesis Co Advisor	Santi Kulprathipanja, Ph.D.

Accepted by the the Petroleum and Petrochemical College, Chulalongkorn University in Partial Fulfillment of the Requirement for the Master of Science

-- Dean of the the Petroleum and
Petrochemical College
(Professor SUWABUN CHIRACHANCHAI, Ph.D.)

THESIS COMMITTEE

-- Chairman
(Professor APANEE LUENGNARUEMITCHAI, Ph.D.)

-- Thesis Advisor
(Professor PRAMOCH RANGSUNVIGIT, Ph.D.)

-- Thesis Co-Advisor
(Santi Kulprathipanja, Ph.D.)

-- External Examiner
(Tanate Danuthai, Ph.D.)

GRAPHICAL ABSTRACT

CH_4

H_2O

SDS

Nonionic surfactant

SDS

Nonionic surfactant/SDS

Hydrate formation

Hydrate dissociation

ชากรณ์ วิริยะกุล : ผลของสารลดแรงตึงผิวต่อการลดการเกิดโฟมเพื่อใช้กับการกัก เก็บแก๊สธรรมชาติด้วยไฮเดรต. (Influence of Mixed Anionic-Nonionic Surfactants on Methane Hydrate Formation: Suppression of Foam Formation) อ.ที่ปรึกษาหลัก : ศ. ดร. ปราโมช รังสรรค์วิจิตร, อ.ที่ปรึกษาร่วม : ดร.สันติ กุลประทีปัญญา

ในปัจจุบันมีความต้องการในการใช้แก๊สธรรมชาติในปริมาณที่สูงขึ้น อย่างไรก็ตามเทคโนโลยีการจัดเก็บและการ ขนส่งแก๊สธรรมชาติในปัจจุบันยังมีข้อจำกัด ส่งผลให้เทคโนโลยีการกักเก็บแก๊สธรรมชาติในรูปแบบของแข็ง (SNG) โดย วิธีไฮเดรตเป็นหนึ่งในเทคโนโลยีที่ได้รับความสนใจในการศึกษาและพัฒนาเพิ่มขึ้น ถึงแม้ว่าเทคโนโลยีนี้จะมีข้อดีหลายประการ เช่น เป็นมิตรกับสิ่งแวดล้อม ปริมาณการกักเก็บแก๊สที่สูง อีกทั้งมีสภาวะในการใช้งานที่ปลอดภัย แต่ผลกระทบเรื่องการเกิดโฟม ในระหว่างการปลดปล่อยแก๊สจากการเติมโซเดียมโดเดซิลซัลเฟต (SDS) เป็นตัวเร่งทางจลน์ในระหว่างการเกิดไฮเดรตทำให้ สารลดแรงตึงผิวหายไประหว่างการนำแก๊สกลับมาใช้งาน ดังนั้นงานวิจัยนี้จึงได้ศึกษาผลของการผสม SDS กับสารลดแรงตึง ผิวแบบไม่มีประจุเพื่อลดปัญหาการเกิดโฟม โดยศึกษาการใช้โพลีออกซีเอทิลลีนลอรีลอีเทอร์ (EO_3 และ EO_5) และอัลคิล โพลีไกลคอล (APG) ผสมกับ SDS ในความเข้มข้นต่างๆ คือ 0.0625/0.25 0.125/0.25 และ 0.25/0.25 เปอร์เซ็นต์โดยน้ำหนักของสารลดแรงตึงผิวแบบไม่มีประจุต่อ SDS ที่ความดัน 8 เมกะปาสคาล และ 4 องศาเซลเซียสใน สภาวะที่ปราศจากการรบกวน ซึ่งผลการศึกษาพบว่าการเติม EO_3 ในความเข้มข้นที่สูงขึ้น ส่งผลให้เวลาเริ่มต้นในการเกิดไฮ เดรตนั้นลดลง ในขณะที่อัตราการเกิดไฮเดรต (NR_{30}) และปริมาณการกักเก็บแก๊สนั้นไม่มีการเปลี่ยนแปลงอย่างมีนัยสำคัญ เมื่อเทียบกับการใช้เพียง SDS นอกจากนั้นปริมาณโฟมที่เกิดขึ้นลดลงตามความเข้มข้นที่เพิ่มขึ้นของ EO_3 ในส่วนของการ เติม EO_5 เวลาที่ใช้ในการเกิดไฮเดรตและ NR_{30} แสดงพฤติกรรมการเกิดไฮเดรตแบบไม่มีแนวโน้มที่แน่นอน และสิ่งที่ น่าสนใจคือการเติม 0.25 เปอร์เซ็นต์โดยน้ำหนักของ EO_5 ส่งผลให้ปริมาณการเกิดโฟมน้อยที่สุดเมื่อเทียบกับทุกสภาวะใน การทดลอง นอกจากนี้การใช้ APG ไม่เพียงแต่ทำให้เวลาในการเกิดไฮเดรตสูงขึ้นแต่ยังทำให้ NR_{30} และปริมาณการกักเก็บ แก๊สลดลง อย่างไรก็ตามการเติม 0.25 เปอร์เซ็นต์โดยน้ำหนักของ APG ส่งผลให้การเกิดโฟมลดลงใกล้เคียงกับ 0.25 เปอร์เซ็นต์โดยน้ำหนักของ EO_5 นอกจากนี้ค่าเฉลี่ยของปริมาณการเกิดไฮเดรตของทุกการทดลองอยู่ที่ 83 เปอร์เซ็น

สาขาวิชา	เทคโนโลยีปิโตรเคมี	ลายมือชื่อนิสิต ....
ปีการศึกษา	2562	ลายมือชื่อ อ.ที่ปรึกษาหลัก ....
		ลายมือชื่อ อ.ที่ปรึกษาร่วม

6171001063 : MAJOR PETROCHEMICAL TECHNOLOGY
KEYWOR
D:

Chakorn Viriyakul : Influence of Mixed Anionic-Nonionic Surfactants on Methane Hydrate Formation: Suppression of Foam Formation. Advisor: Prof. PRAMOCH RANGSUNVIGIT, Ph.D. Co-advisor: Santi Kulprathipanja, Ph.D.

Solidified natural gas (SNG) via clathrate hydrate is a new technology for natural gas storage with high energy content per unit volume, extremely safe, and ease to recover. Although SNG has several advantages, its limitation is low rate of hydrate formation. Sodium dodecyl sulfate (SDS) is well known as a kinetic promoter used to increase the hydrate formation rate. However, using SDS resulted in a large amount of foam during gas recovery. In order to alleviate this problem, mixtures of SDS with nonionic surfactants were investigated. Polyoxyethylene (n) lauryl ether (EO_3 and EO_5) and alkyl poly glycol (APG) were mixed with SDS in different concentrations for the formation at 8 MPa and 4 ℃ in the quiescent condition. The experiment was investigated for the effects of these mixed surfactants in both kinetics and morphology studies. The result showed that the addition of EO_3 resulted in the gradual increase in the induction time with the addition of higher concentration of EO_3, while there was no difference for the NR_{30}. Adding EO_5 showed the stochastic phenomenon on the induction time and NR_{30}. In the presence of APG, the induction time increased up to ten times, while the NR_{30} was lowered compared to only 0.25 wt% SDS. Interestingly, there was no significant different on the methane uptake with all conditions. The morphology showed similar hydrate formation and dissociation patterns with all investigated solutions. However, the different foam height at 8 hr was observed. The addition of EO_3 showed a gradual decrease in the foam formation with the higher concentration of EO_3. Adding the highest EO_5 concentration showed the optimum foam reduction compared with all conditions, while lower concentration cannot lower the foam generated. Moreover, the presence of APG showed the similar effects of foam reduction with EO_5. Furthermore, all experiments maintained the average hydrate yield and the amount of gas recover as 83 and $\geq$ 90%, respectively.

Field of Study:	Petrochemical Technology	Student's Signature
		....
Academic Year:	2019	Advisor's Signature
		....
		Co-advisor's Signature
		....

ACKNOWLEDGEMENTS

TABLE OF CONTENTS

LIST OF TABLES

LIST OF FIGURES

CHAPTER 1
INTRODUCTION

Natural gas tops the list of the most used energy sources because it is highly combustible, extremely safe, and cleaner than other forms of energy (Siangsai *et al.*, 2015; Veluswamy *et al.*, 2016b). These reasons result in the increasing global demand for natural gas. There is an increase need to develop technologies to store natural gas on a large scale. Natural gas can be stored in the form of compressed natural gas (CNG), liquified natural gas (LNG), and adsorbed natural gas (ANG) (Lozano-Castelló *et al.*, 2002). For CNG, natural gas is stored at a high pressure. Although CNG has been widely used, the volumetric storage capacity, and the safety are still the issues. LNG has a problem on boil-off gas (BOG) because the temperature used to store natural gas is -162 °C. LNG also requires expensive equipment to maintain natural gas in the liquid form (Sapag *et al.*, 2010; Sun *et al.*, 1997). ANG uses adsorbents including activated carbon, graphene, and metal organic frameworks (MOFs), to increase the storage capacity. However, the heat generation during adsorption and desorption affects the storage performance. Solidified natural gas (SNG) technology via gas hydrates has emerged as a potential natural gas storage candidate. The technology involves low temperature and high pressure to store natural gas with potential for large scale storage of natural gas (Veluswamy *et al.,* 2018).

Gas hydrates or clathrate hydrates are solid ice like, non-stoichiometric compounds. The small guest gas molecule (methane, ethane, etc.) is trapped inside the hydrogen bonded water cages (Koh *et al.*, 2011; Sloan and Koh, 2008). The physical interaction between the guest gas and water cages is Van der Waals forces to stabilize the structure (Veluswamy *et al.,* 2017). The suitable thermodynamic conditions and size of guest gas molecules allow gas hydrates to form three common crystal structures; cubic structure I and II (sI and sII) and hexagonal structure H (sH). One volume of solid methane hydrates can store about 150-180 volume methane gas at STP (Sloan, 2003). This characteristic feature of natural gas hydrates is favorable for transporting and storing natural gas in large quantities (Hao *et al.*, 2008). The storage of natural gas in the hydrates form has several advantages that include environmentally benign, guest gas can almost completely for recovered by simple

depressurization or thermal stimulation, moderate temperature and pressure conditions are required during hydrate formation and storage process. (Kumar *et al.*, 2019; Veluswamy *et al.*, 2017; Veluswamy *et al.*, 2016b).

Although the gas hydrate technology for storage natural gas has several advantages, it has kinetics limitation with slow rate of hydrate formation. Using a kinetics promoter is one way to alleviate this problem by accelerating the hydrate formation, improving the volumetric storage capacity, and reducing hydrate induction time (Khurana *et al.*, 2017; Siangsai *et al.*, 2015). An anionic surfactant, especially sodium dodecyl sulfate (SDS), has been reported to be the best kinetics promoter due to the presence of SDS surfactant decreases interfacial surface tension between the gas/liquid phase and improves the mass transfer of guest gas molecules to the liquid phase (Lin *et al.*, 2004; Zhang *et al.*, 2007). However, the disadvantage of SDS as the hydrate kinetics promoter is a large amount of foam generated during the dissociation process to recover the stored gas. Silicone has been added as an antifoam agent. It has been used to retain the properties of SDS and preventing foam formation, while it does not affect the gas capacity (Bhattacharjee *et al.*, 2017). Using surfactant mixtures (e.g., anionic/nonionic surfactant mixtures) can be attained to reduce anionic head group. SDS works with a nonionic surfactant has been proposed to suppress the foam formation during the hydrate formation and dissociation, while it still keeps the higher rate of formation in the mixed system.

In this work, the objective was to suppress the excessive foam formation during the hydrate dissociation. This work used SDS surfactant as a kinetics promoter with a nonionic surfactant. The SDS and a nonionic surfactant was mixed in various concentrations in order to find the optimal ratio for the two additives and the gas uptake. Hydrate formation was carried out in an unstirred tank reactor system. Pressure and temperature conditions for hydrate formation was 8.0 MPa and 4 ℃, respectively.

CHAPTER 2
LITERATURE REVIEWS

2.1 Natural Gas

Natural Gas is primarily methane (CH_4) with smaller quantities of other forms of hydrocarbons such as ethane, propane etc. It was formed millions of years ago when dead marine organisms sunk to the bottom of the ocean and were buried under deposits of sedimentary rock. Subject to intense heat and pressure, these organisms underwent a transformation, from which they were converted to a gas over millions of years. Natural gas is found in underground rock called reservoirs. The rocks have tiny spaces in them (called pores) that allow them to hold water, natural gas, and oil. Nowadays, there are many uses of natural gas, some of which include electricity generation, transportation, and manufacturing. Even though natural gas is non-renewable energy but many uses for natural gas have increased because it can reduce pollution and benefit from economic, public health, and environmental benefits (Speight, 2008).
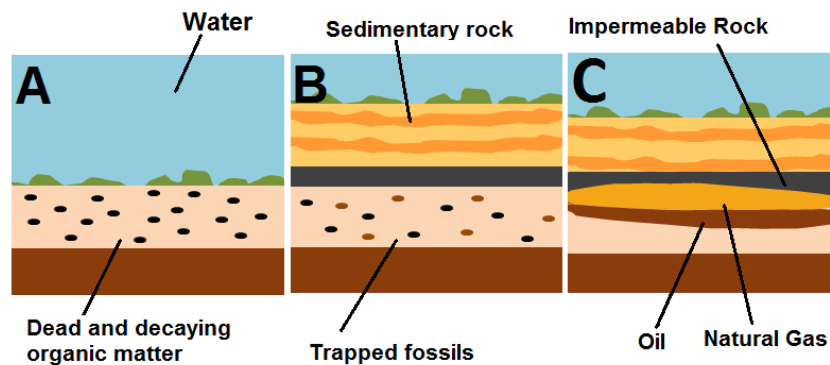
Figure 2.1 Petroleum and natural gas formation (EIA, 2018).

2.2 Natural Gas Storage

In recent years, natural gas has gained more attention in terms of green alternative energy. The exploration, production, and transportation of natural gas always take time in the process. Natural gas that reaches its destination is not always needed right away. For this reason, natural gas storage facilities are essential to support the increasing global demand of technology (Veluswamy *et al.*, 2018).

2.2.1 Compress Natural Gas (CNG)

CNG is alternative energy, which includes methane as the main composition. CNG is stored in the condition of high pressure around 20-25 MPa (200 to 250 bars, or 3,000 to 3,600 psi). The use of CNG as a transport fuel is a mature technology. It is usually used in a small fuel place. Although compressed natural gas is a fossil fuel, it is the cleanest burning fuel at the moment.

2.2.2 Liquefied Natural Gas (LNG)

LNG is natural gas that has been cooled to liquid state. Gas is converted to liquid form at -162 °C. LNG can reduce cost for transport facilities, and it offers energy density similar with diesel fuel. However, it needs to store in a storage tank, which is specially designed to maintain the temperature required to keep LNG in the liquid form and required the expensive equipment to maintain the system.

2.2.3 Adsorbed Natural Gas (ANG)

In ANG, natural gas is trapped inside highly porous materials as adsorbents under standard condition. ANG uses adsorbents including activated carbon, graphene or metal organic frameworks (MOFs), etc, for increasing the storage capacity.

Another means of storage gas by using porous material is solidified natural gas (SNG) via gas hydrates. This technology turns natural gas into the hydrate form. The guest gas molecule (methane, ethane, etc.) is trapped inside the water cages. Gas

hydrates may be able to meet global demand for natural gas storage because the storage condition involves low to moderate temperature and not high pressure as other methods.

2.3 Gas Hydrates

Gas hydrates or clathrate hydrates are solid ice like, non-stoichiometric compounds. Natural gas (guest molecule) is trapped inside the hydrogen bond water cages (host molecule), and the guest molecule interacts with water molecules through Van der Waals forces to stabilize the structure. Gas hydrates involve low temperature and high pressure to store natural gas with potential for large scale storage of natural gas (Babu *et al.*, 2015). In the past, gas hydrates have been considered as a problem during exploration and production in industries. They disrupted the operation in the gas pipeline during the gas production resulting in large loss (Veluswamy *et al.*, 2018). However, gas hydrates have emerged as an alternative technology in order to use for many applications, including natural gas storage and transportation, gas separation, and sea water desalination.

Figure 2.2 Methane will ignite in ice form (Discover, 2014).

Gas hydrates are composed of three main clathrate repeating crystal structures: I, II and H. The type of hydrate that forms depends mainly on the molecular diameters of the gas molecules and gas hydrate formation condition (Gabitto and Tsouris, 2010).

1. Structure I or sI, a body-centered cubic structure. Gas hydrates can hold small gas molecules (0.4–0.55 nm), like natural gas containing molecules smaller than propane; accordingly, sI hydrates are found in situ in deep oceans with biogenic gases containing mostly methane, carbon dioxide, and hydrogen sulfide.

2. Structure II or sII, a diamond lattice within a cubic framework. Gas hydrates can maintain relatively large molecules (0.6–0.7 nm), like natural gas or oil containing molecules larger than ethane but smaller than pentane. sII represents hydrates from thermogenic gases.

3. Structure H or sH gas hydrates only contain mixtures of large and small molecules (0.8-0.9 nm) such as methyl cyclohexane and methane. The volume of methane occupying small and medium cages formed using sH promoter is shown to have highest volume than sI and sII hydrate structures.
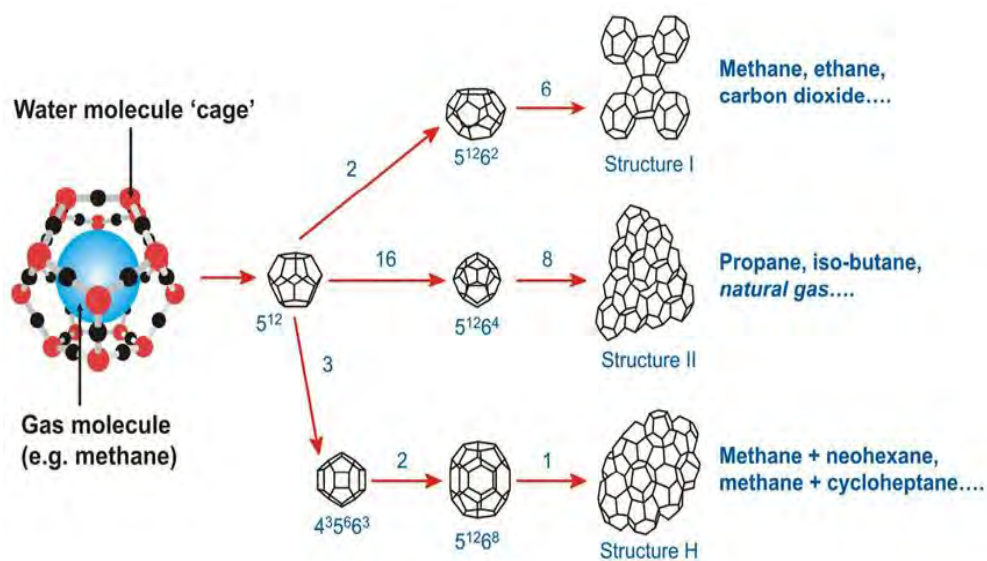
Figure 2.3 Structure types of gas hydrates (Jones *et al.*, 2010).

Figure 2.3 shows the three main common structure types, cavity types, and guest molecules. The symbol $5^{12}6^2$ specifies a water cage composed of twelve pentagonal and two hexagonal faces. The number in squares means the number of cage types. For example, the structure I unit crystal is composed of contain 46 water molecules per 8 gas molecules consisting of 2 small and 6 large cages. The properties of different hydrate structures are shown in Table 2.1

Table 2.1 Properties of different hydrate structure (Sum *et al.*, 1997)

Cavity	I		II		H		
	small	large	small	large	small	medium	large
description	5^{12}	$5^{12}6^2$	5^{12}	$5^{12}6^4$	5^{12}	$4^35^66^3$	$5^{12}6^8$
no. of cavities unit cell	2	6	16	8	3	2	1
av cavity radius, A	3.95	4.33	3.91	4.73	3.91	4.06	5.71
variation in radius, %	3.4	14.4	5.5	1.73	not available		
coordination number	20	24	20	28	20	20	36
no. of waters/unit cell	46	-	136	-	34	-	-

2.4 Gas Hydrate Formation

Gas hydrate formation is a crystallization process. When structure of water cage is formed, guest gas molecules will be trapped inside the water cage at appropriate temperature and pressures. Figure 2.4 provides a schematic representation of the hydrate formation steps. Starting with gas dissolve into water, hydrate nucleation, and hydrate growth, upon successful hydrate nucleation, a thin hydrate film forms on water gas interface, which continues in the mass transfer of guest gas molecule to liquid phase. Solubility of hydrates formed and contact area between the hydrates and water have been used to observe to ensure the hydrate growth (Yin and Linga, 2019).

- Dissolution

Gas dissolution occurs after gas is fed into the system. The gas will dissolve from the gas phase to the liquid phase, before it is continuously dissolved into the solution until the solution reaches the saturated point (Posteraro *et al.,* 2016).

- Hydrate Nucleation

Hydrate nucleus is like a small cluster, which is combined between gas and water molecules. It initiates at the gas/liquid interface and continues to form until it reaches the critical point of hydrate nucleation step (Posteraro *et al.*, 2016).

- Hydrate Growth

Hydrate growth occurs after the hydrate nucleation step. The growth process takes places until it reaches the complete form of the gas hydrates. The important factor in the process is the heat and mass transfer between gas hydrate molecule and solution (Kang *et al.*, 2016).
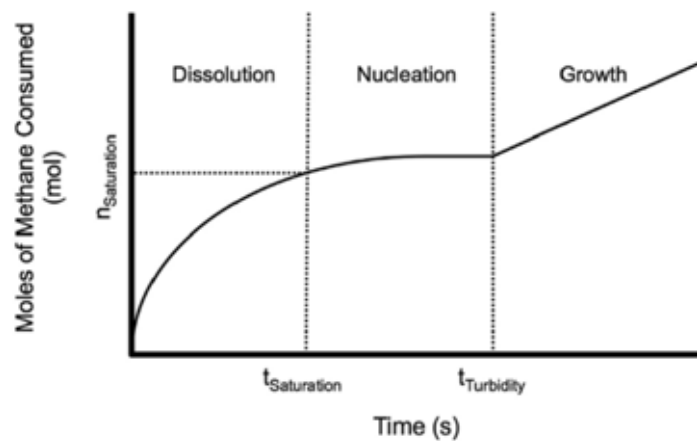
Figure 2.4 Representation of three phases of hydrate formation in terms of gas consumption (Posteraro *et al*., 2016).

2.5 Hydrate Dissociation

Hydrate dissociation is the elimination of hydrate crystal. The decomposition of the gas hydrates occurs through breaking hydrogen bond water cages, Van der Waals interaction between guest gas molecules and water cages (Sloan and Koh, 2008). Method that used to do hydrate dissociation are include Thermal stimulation, pressure reduction and chemical injection.

- Thermal Stimulation

Dissociation of hydrates can be promoted through heat the system above phase equilibrium.

- <u>Pressure Reduction</u>

Dissociation of hydrates can be promoted through the reduction pressure in the system below phase equilibrium.

- <u>Chemical Injection</u>

Methanol or glycol injection can be used to break down the hydrates. The conditions, under which this is appropriate strategy, depends on the positioning of the hydrates as the injected fluid must have direct contact with the hydrate formation.

2.6 Surfactants

Surfactants are substances that create self-assembled molecular clusters called micelles in a solution (water or oil phase) and adsorb to the interface between a solution and a different phase (gases/solids). To show these two physical properties, a surfactant must have a chemical structure with two different functional groups with different affinity within the same molecule. Usually the molecules of the substances called surfactants have both an alkyl chain with 8-22 carbons. This chain is called a hydrophobic group, which does not show affinity to water (they are called hydrophobic groups since surfactants are often used in water systems, but when used in lipid systems they are called lipophilic groups). The surfactant molecules also have a functional group called the hydrophilic group that has affinity to water. This kind of structure with two opposing functions is called an amphiphilic structure. Figure 2.5 shows the classification of surfactants, which include anionic surfactant, cationic surfactant, nonionic surfactants, and zwitterionic surfactant (Rhein, 2007).
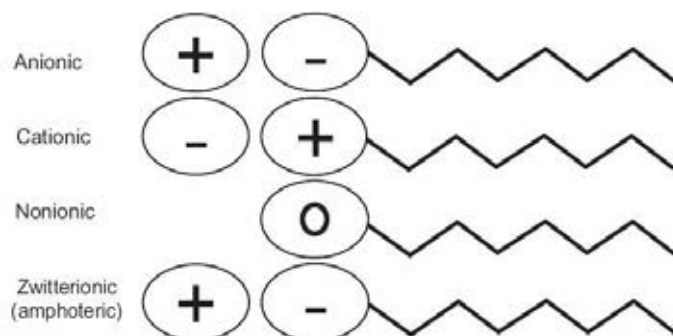
Figure 2.5 Structure and classification of surfactants (Som *et al.*, 2011).

Surfactants are also classified depending on their solubility, such as hydrophilic surfactants that are soluble in water or hydrophobic (lipophilic) surfactants that are soluble in lipids. Ionic surfactants are generally hydrophilic surfactants, but nonionic surfactants can be either hydrophilic or lipophilic, depending on the balance of the hydrophilic group and lipophilic group. Hydrophilic-lipophilic balance (HLB) is an indicator that quantifies the relative balance, which is shown in Figure 2.6. It is commonly used as an indicator for choosing a surfactant for specific applications.
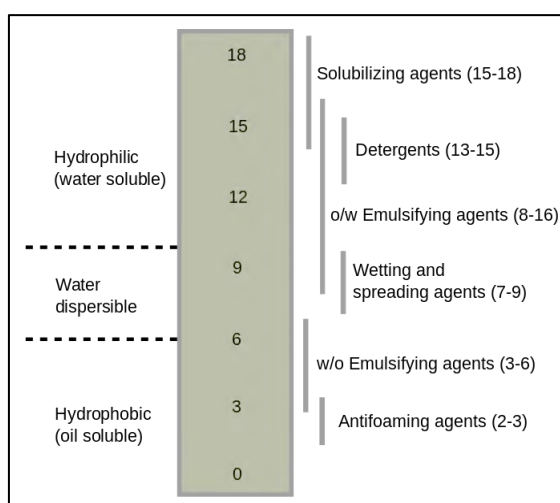
Figure 2.6 Index for choosing surfactants (Wikiwand, 2018).

When the concentration of a solution is higher than the critical micelle concentration (CMC), micelles and monomolecular surfactants (monomers) coexist in the aqueous solution and in the solution. They keep a dynamic equilibrium as they associate and dissociate. The exchange rate of the dynamic equilibrium is reported to be of the order of microseconds. Simple micelles are often depicted as being spherical, with disorderly aligned alkyl chains filling the core and with a rough surface with a liquid property. The Krafft point is the temperature, at which the solubility of ionic surfactants in water increases. It is defined as the triple point of the surfactant monomer's solubility curve, the CMC temperature curve, and the phase transition line (Tc) of hydrated solids to micelles and/or liquid crystal. When the surfactant solution is lower than its Krafft point and higher than the CMC, it forms a bilayer structure hydrated solid, and if it is higher than its Krafft point and higher than the CMC, it forms micelles, as shown in Figure 2.7.
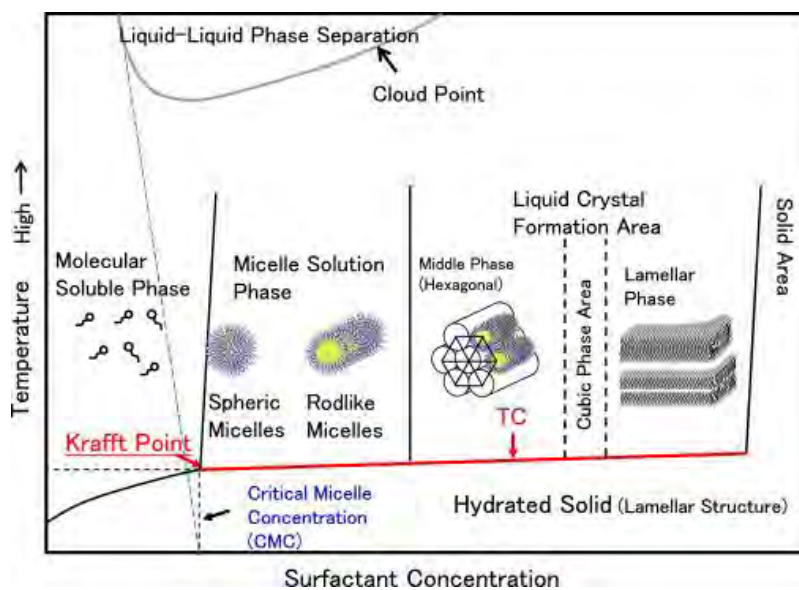
Figure 2.7 The concentration and temperature dependency of the phase conditions of a surfactant aqueous solution (Nakama, 2017).

2.7 Anionic Surfactants

Anionic surfactant is a surface active substance that contains wash active and degreasing abilities on the surfaces of metals (Rhien, 2007). It lowers the surface tension of water and thus removes the dirt from the surfaces of the metals. In an anionic surfactant, the hydrophilic part consists of negatively charged group. Anionic surfactants are all surfactants that carry a negatively charged head group (Lin *et al.*, 2004).

- Sodium Dodecyl Sulfate (SDS)

SDS is a synthetic organic compound with the formula structure $CH_3(CH_2)_{11}SO_4Na$. It is an anionic surfactant which used in many cleaning and hygiene products. The sodium salt is of an organo sulfate class of organics. It consists of a 12 carbons tail attached to a sulfate group. It is the sodium salt of dodecyl hydrogen sulfate (SDS), the ester of dodecyl alcohol and sulfuric acid. It hydrocarbon tail combined with a polar ,headgroup, give the compound amphiphilic properties and so make it useful as a detergent. Figure 2.8 shows the structure of SDS.
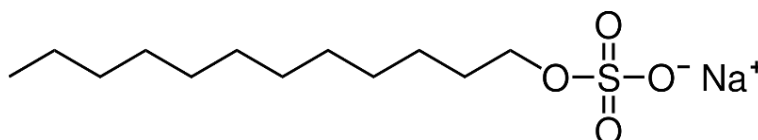
Figure 2.8 Structure of SDS.

- Sodium Tetradecyl Sulfate (STS)

STS is an organic sodium salt having tetradecyl sulfate as the counterion with formula structure $C_{14}H_{29}NaO_4S$. Used in the treatment of small uncomplicated varicose veins of the lower extremities that show simple dilation with competent valves. It has a role as a detergent and a sclerotherapy agent. It contains a tetradecyl sulfate (Yoslim *et al.*, 2010). Figure 2.9 shows the structure of STS.
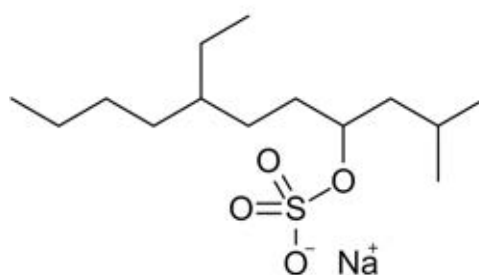
Figure 2.9 Structure of STS.

- Sodium Hexadecyl Sulfate (SHS)

Sodium tetradecyl sulfate is an organic sodium salt having tetradecyl sulfate as the counterion. Used in the treatment of small uncomplicated varicose veins of the lower extremities that show simple dilation with competent valves. It has a role as a detergent and a sclerotherapy agent. It contains a tetradecyl sulfate (Yoslim *et al.*, 2010). Figure 2.10 shows the structure of SHS.
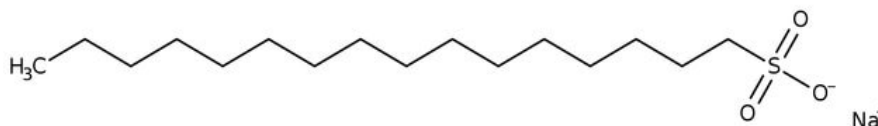
Figure 2.10 Structure of SHS.

2.8 Nonionic Surfactants

Nonionic surfactants are widely used in technical applications such as detergency, emulsification, cosmetics, and defoamer. It consists of hydrophobic as a tail group with a length of carbons and hydrophilic as a headgroup with ethylene oxide units. The technology related to depress foam formation mostly uses a nonionic surfactant as a defoamer (Rhien, 2007). Gas hydrate technology has used anionic surfactant to accelerate the hydrate formation, improving the volumetric storage capacity and reducing hydrate induction time but a large amount of foam generated. Adding nonionic surfactant, they will be placed between anionic surfactant to reduce

electrostatic repulsion, which resulting in reduce foam generation (Kumar *et al.*, 2015).

Aqueous solutions of nonionic surfactants exhibit low foaming above their cloud point, a temperature above which the homogeneous solutions separate into two phases: a dilute phase containing a low surfactant concentration and coacervate phase containing a very high surfactant concentration (e.g., 20 wt% surfactant) (Chaisalee *et al.*, 2003).

EOs are a class of compounds that are commonly used throughout many industrial practices and commercial markets. These compounds are synthesized via the reaction of a fatty alcohol and ethylene oxide, resulting in a molecule that consists of two main components, the oleophilic, carbon-rich, fatty alcohol and the hydrophilic, poly oxyethylene chain which is shown in Figure 2.11.
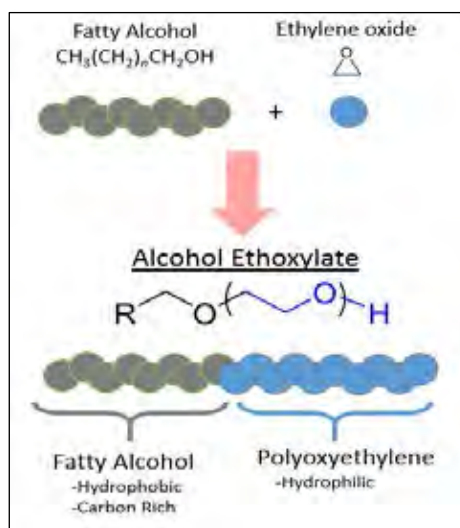
Figure 2.11 Show alcohol ethoxylate structure (Oxiteno, 2018).

2.9 Foam

Foam are a special kind of colloidal dispersion. It is formed by trapping of gas in liquid or solid. Gas is dispersed in liquid phase called "continuous liquid phase". The disperse phase is sometime to called as the internal phase, and the continuous phase is called as the external phase. Foams have long been known and interest

because of their widespread occurrence in daily life. It has an important property which will be desirable product such as fire-extinguishing and has undesirable product such as foam in an industrial distillation tower. When foams are generated in variety of the process often may create major loss from the economically consequences of uncontrolled foaming can be significant. However, many drawbacks from foam generation process still on the way to find the way to solve. De-foaming or antifoaming agents has been proposed to depress the foam generated during the operating process (Nakama, 2017).

2.10 Defoamers and Anti-foaming Agents

A defoamer or anti-foaming agent is chemical additive added to the system which used to prevent the foam formation, hinder the entrainment of a gas in a liquid, or to break a foam that previously formed. They are necessary in various industrial and are the important factor to get the optimum efficient operation. At high bulk viscosity, lowering the surface tension is not relevant for the mechanism of stabilization of foams, but for all other mechanisms of foam stabilization a change of the surface properties is essential. A defoaming agent will change the surface properties of a foam upon activation (McClure *et al.*, 2017).
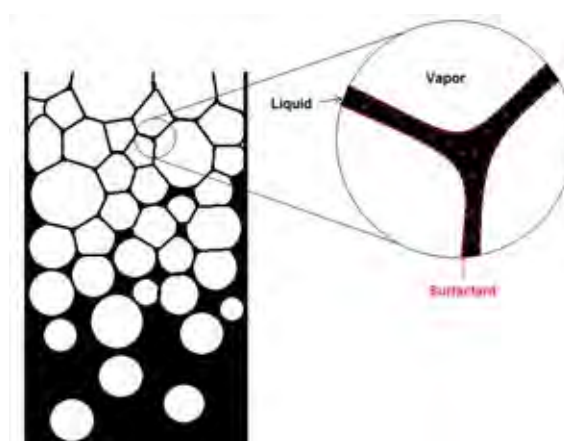
Figure 2.12 the accumulation of surfactant molecules at liquid-vapor interface (https://en.wikipedia.org/wiki/Continuous_foam_separation).

Figure 2.12 shown the position of surfactant molecules at liquid-vapor interface which is used as a defoamers in the column. In the presence of defoamer reduced the electrostatic repulsion between thin film resulting in gas bubble breaking.

Kalogerakis *et al.* (1993) investigate experimentally the effect of surfactants on the formation kinetics of methane hydrate which include anionic, cationic, nonionic surfactants. The results show that the liquid mass transfer coefficient decrease by about 50% due to the presence of the surfactants. The effect is more pronounced with anionic surfactants compared to nonionic and cationic.

Ganji *et al.* (2007) study effect of different type of surfactant, which include anionic surfactant, cationic surfactant, and nonionic surfactant. In the presence of every surfactant, the amount of gas storage in term of storage capacity was increase higher than only water as show in Figure 2.13. Although in the presence of surfactant increase the storage capacity but only anionic surfactant significantly decreased the induction time of hydrate formation so anionic surfactant has been reported on of the best kinetic promotor especially sodium dodecyl sulfate (SDS).
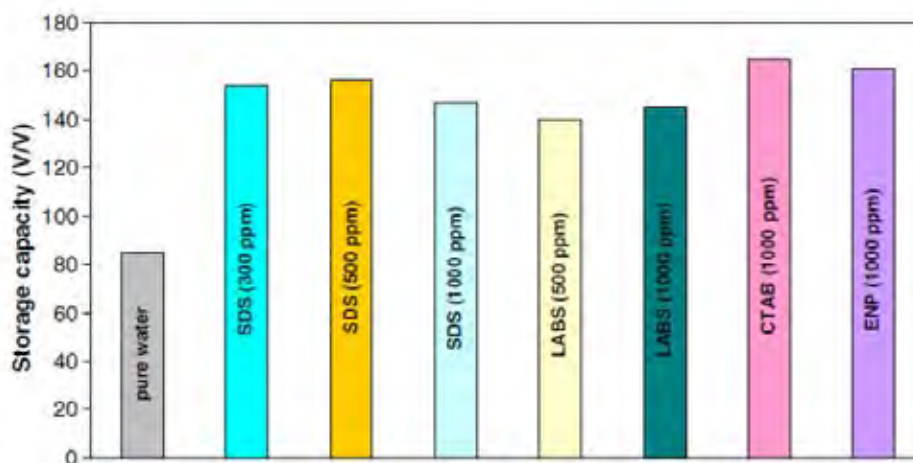
Figure 2.13 Storage capacity of hydrate formed with and without promoters.

Yoslim *et al.* (2010) study effect of three commercially available anionic surfactants on the hydrate growth, which include sodium dodecyl sulfate (SDS), sodium tetradecyl sulfate (STS), and sodium hexadecyl sulfate (SHS). The result in the presence of SDS show the highest amount of gas uptake.

Bhattacharjee *et al.* (2018) investigated the additional of sodium dodecyl sulfate (SDS) can solve the limitations of the slow rate of hydrate formation. SDS used to alleviate this problem by accelerating the hydrate formation, improving the volumetric storage capacity and reducing hydrate induction time. However, using SDS as a kinetics promoter also have the large amount of foam generated, affected to losing gas recover capacity. Silicone based surfactant has been proposed to be used as antifoam in conjunction with SDS to prevent the foam generation during hydrate formation and hydrate dissociation. Figure 2.14 shows the comparison of the gas uptake and Figure 2.15 shows the average rate of gas uptake for the different systems studied.
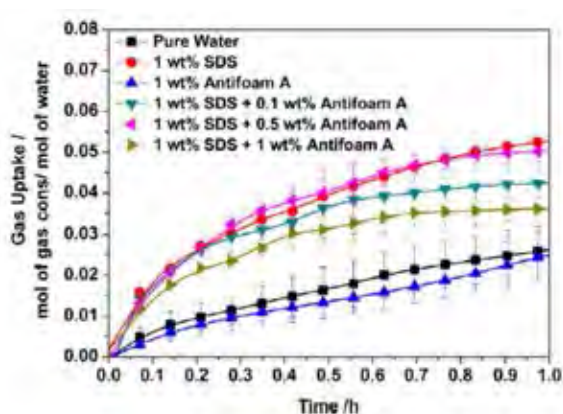
Figure 2.14 Comparison of the gas uptake for the different systems studied with average and standard deviation (Bhattacharjee *et al.*, 2018).
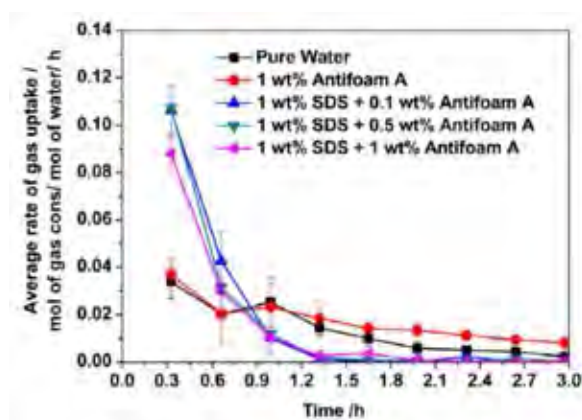
Figure 2.15 Average rate of gas uptake for the different systems studied with standard deviation (Bhattacharjee *et al.*, 2018).

Therefore SDS-Silicone complexes were formed by combining two additives (anionic surfactant SDS and silicone surfactant antifoam). These complexes are supposed to retain the various properties of SDS while also having reduced surface tension and increased hydrophobicity as compared to pure SDS. it can be concluded that the 1 wt% SDS + 0.5 wt% Antifoam-A system performs the best in terms of enhancing the kinetics of methane hydrate formation and the hydrate formation kinetics observed with this system were on par with those observed with pure SDS.
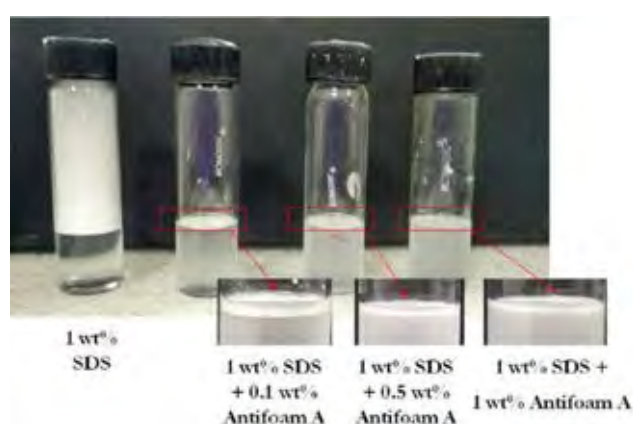
Figure 2.16 Foam suppression in presence of silicone base surfactant (Bhattacharjee *et al.*, 2018).

Pandey *et al.* (2018) study the approaches to alleviate foam formation is the use of various antifoaming agents which may be employed in combination with surfactants. The possibility of using one such antifoaming agent, a silicone based polymeric surfactant, for hydrate base methane storage, has been explored in this work through a detailed morphological.
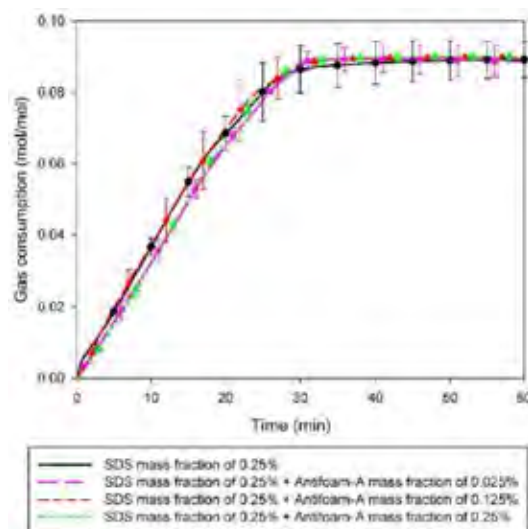
Figure 2.17 Comparison of gas uptake during the methane hydrate formation (Pandey *et al.*, 2018).

Table 2.2 Summary of all experiments (Pandey *et al.*, 2018)

exp no.	system additive (mass fraction %)	soln state	soln vol (mL)	initial pressure (MPa)	initial temp (K)	final gas uptake (mol/mol)
1	SDS (0.25)	fresh	5	6.1	274.55	0.088
2	SDS (0.25)	memory	5	6.1	274.25	0.090
3	SDS (0.25) + Antifoam A (0.025)	fresh	5	6.1	274.35	0.084
4	SDS (0.25) + Antifoam A (0.025)	memory	5	6.0	274.48	0.086
5	SDS (0.25) + Antifoam A (0.125)	fresh	5	6.0	274.55	0.089
6	SDS (0.25) + Antifoam A (0.125)	memory	5	6.1	274.55	0.090
7	SDS (0.25) + Antifoam A (0.25)	fresh	5	6.0	274.53	0.093
8	SDS (0.25) + Antifoam A (0.25)	memory	5	6.1	274.55	0.088

The system with 1:0.5 (in terms of mass fraction) SDS:antifoam ratio, the kinetics of methane hydrate formation obtained was slightly faster than that for the pure SDS system. Silicone based antifoam thus demonstrated no negative effects on the kinetics of methane hydrate formation and necessitates the requirement of an optimum SDS:antifoam ratio in order to achieve desired antifoaming activity.
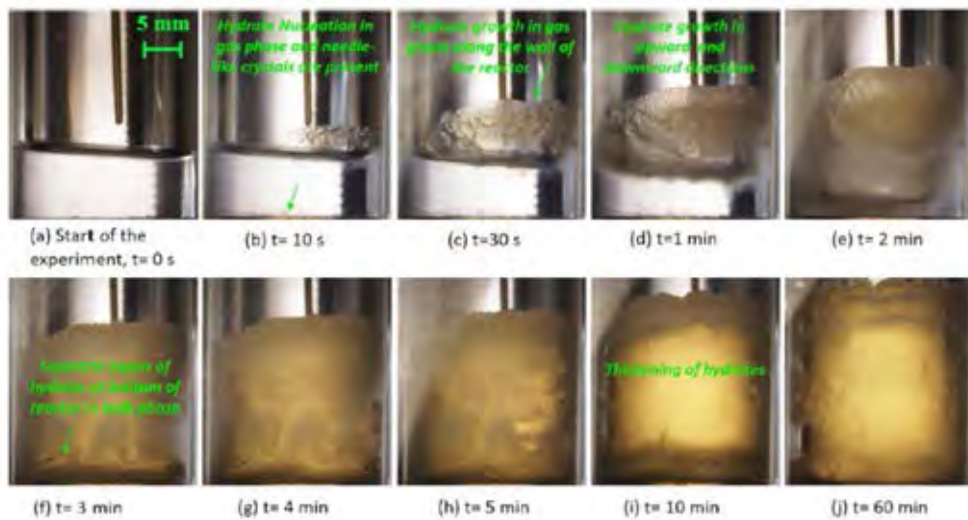
Figure 2.18 Morphology images of methane hydrate formation (Pandey *et al.*, 2018).
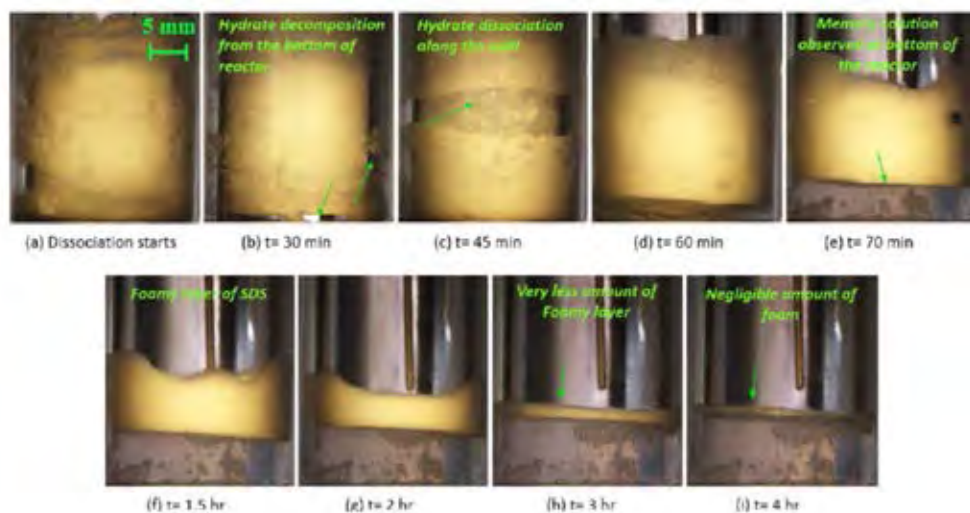
Figure 2.19 Morphology images of methane hydrate dissociation (Pandey *et al.*, 2018).

Rhein (2007) reported the detergency of nonionic surfactants is equal to, and in many cases better than, that of anionic detergents. Ethylene oxide (nonionic surfactant) as long chain ethoxylated alcohols are another type of nonionic surfactants but can have serious flash foam and foam volume issues.

McClure *et al.* (2017) in this experiment study the comparison between two type of antifoam agent (silicone surfactant and nonionic surfactant) on oxygen transfer rate (OTR). They were found that antifoams examined behaved similarly in

terms of OTR reduction. In term of percentage rise of foam generation in the presence of antifoams, for nonionic at high concentration enough the percentage rise of foam formation is lower than silicone surfactant. They were also found that silicone surfactant is faster to deactivate than nonionic surfactant.
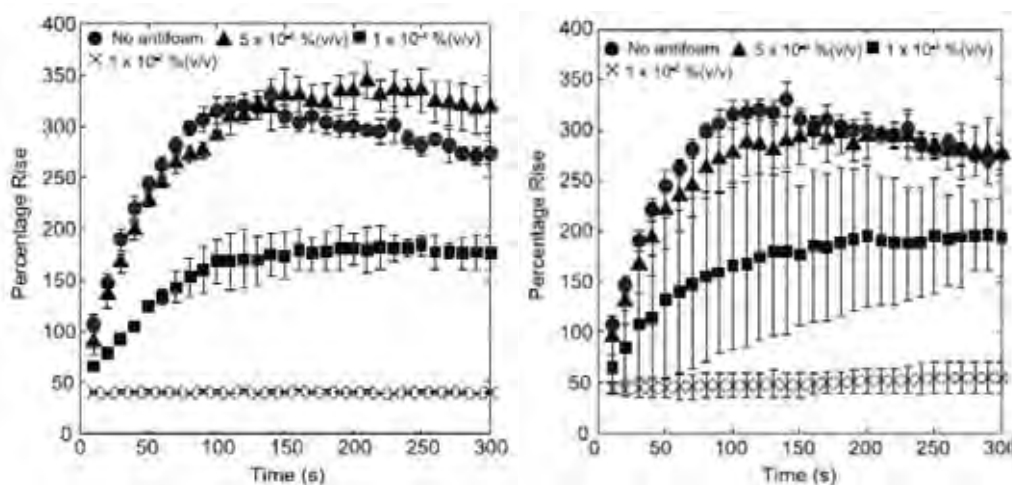
Figure 2.20 plot showing the percentage rise of the foamlayer as a function of time (McClure *et al.*, 2017).

Chaisalee *et al.* (2003) reported the aqueous solutions of nonionic surfactants exhibit low foaming above their cloud point, a temperature above which the homogeneous solutions separates into two phases: a dilute phase containing a low surfactant concentration and coacervate phase containing a high surfactant concentration (e.g., 20 wt% surfactant). Figure 2.21 shows the schematic of phase separation when the temperature is increasing.
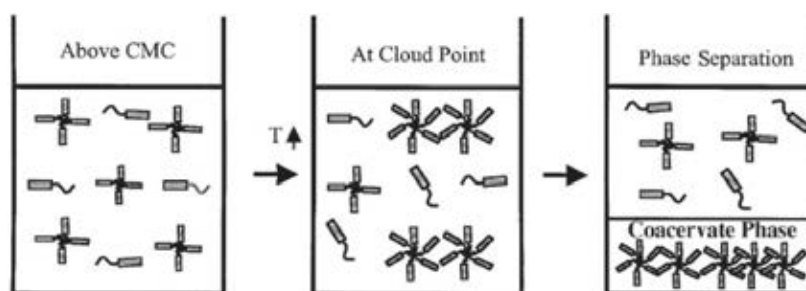
Figure 2.21 Schematic of phase separation (Chaisalee *et al.*, 2003).

CHAPTER 3
METHODOLOGY

3.1 Materials and Equipment

3.1.1 Equipment

Hydrate formation/dissociation apparatus

1. Crystallizer (CR)
2. Reservoir (R)
3. Personal computer (PC)
4. Pressure transducer (PT)
5. K-type thermocouple
6. Controllable water bath

3.1.2 Chemicals

1. Ultra-high purity methane gas (99.99% purity from Linde Public Company, Thailand)
2. Sodium dodecyl sulfate (Bio Xtra grade, >99.0% purity (GC) from Sigma- Aldrich, Japan)
3. Polyoxyethylene (3) Lauryl ether (>99.7% purity from Thai Ethoxylate Company Limited, Thailand)
4. Polyoxyethylene (5) Lauryl ether (>99.7% purity from Thai Ethoxylate Company Limited, Thailand)
5. Alkyl polyglycol ether (Sasol Chemical Company, USA)
6. Deionized water

3.2 Experimental Apparatus for Kinetics Investigation

The schematic diagram of the gas hydrate experimental setup is shown in Figure 3.1 (left side). The experiment apparatus consists of stainless steel crystallizer, which can withstand up to 20 MPa and has volume of 180 cm^3. The crystallizer was connected with a 100 cm^3 reservoir. Both crystallizer and gas reservoir were immersed in a cooling bath. An external refrigerator (Model RC-20, Daeyang, Korea) circulated the cold fluid (the water and glycol mixing in the ratio of water to glycol is 4:1) was used to maintain the crystallizer temperature. The pressure transmitter (Cole-Pamer®, Singapore) was used to measure the pressure in the system with the range of 0-21 MPa with 0.13 % global error. Figure 3.1 (right side) shows the cross-section of the morphology crystallizer. There were three K-type thermocouples placed in different locations inside the crystallizer with an accuracy ±1.0 ℃. Thermocouples T1, T2, and T3 were placed at the solution phase (bottom), middle phase, and gas phase (top), respectively. The pressure and temperature during the experiment were record by a data logger (AI210, Wisco Industrial Instruments, Thailand), which was connected to a computer.
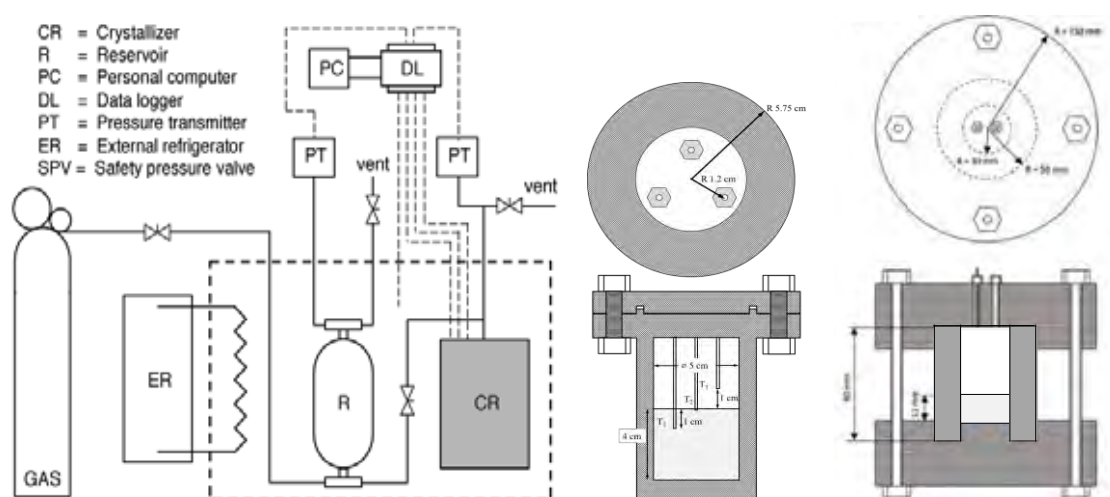
Figure 3.1 Schematic of experimental apparatus (left side) and cross-section of a crystallizer (right side). Modified from Siangsai *et al*. (2015).

3.3 Experimental Apparatus for Morphology Investigation

A detailed description of the experimental apparatus is available in the study by (Veluswamy *et al.*, 2016a); Veluswamy *et al.* (2016c). The reactor column was made of transparent sapphire supported by two stainless steel lids. The reactor had an inner diameter of 30 mm, height of 80 mm, and was designed to withstand 10 MPa pressure. The temperature and pressure in the reactor were measured by a K-type thermocouple with an accuracy ± 1.0 ℃. and the pressure transmitter (Cole-Pamer®, Singapore) in the range of 0−21 MPa respectively. The temperature in the water bath was controlled by an external refrigerator (Model RC-20, Daeyang, Korea). Temperature and pressure during the hydrate formation and dissociation was recorded every 10 s by using a data acquisition system supplied by record by a data logger (AI210, Wisco Industrial Instruments, Thailand), which was connected to a computer.

The images of hydrate formation and dissociation were captured every 10 s by using adjustable magnification telecentric zoom lens from Navitar with Optika C-HP camera.

3.4 Hydrate Formation Experiment

Experimental procedures adopted for kinetics and morphology studies was calculated based on the volume of mixture of 0.25 wt% SDS and different EO_n concentrations and mixture of 0.25 wt% SDS and APG different concentrations. The procedure was similar for both studies except for the sample volumes. 90 mL of the solution was added into the stainless steel crystallizer for the kinetics study whereas 7 ml of the solution was added into the transparent sapphire crystallizer. The crystallizer was pressurized to 0.5 MPa by methane gas and depressurized to atmospheric twice to remove the residual air in the system. The experimental temperature was set at 4 ℃. After this, methane gas was introduced into the crystallizer to 8 MPa. The data was recorded every 10 s for the kinetic experiment and 30 s for the morphology experiment by the data logger. During the hydrate formation, the pressure in the crystallizer decreased due to the hydrate formation. The experiment continued until there was no further pressure drop for at least 1 h. The number of the moles of

methane gas consumed and the methane gas uptake during the hydrate formation at given any time (*t*) were calculated employing equations (3.1) and (3.2):

$$\Delta n_{H,\downarrow} = n_{H,0} - n_{H,t} = \left(\frac{PV}{zRT}\right)_{G,0} - \left(\frac{PV}{zRT}\right)_{G,t} \tag{3.1}$$

$$\text{Methane gas uptake} = \frac{\left(\Delta n_{H,\downarrow}\right)_t}{n_{H_2O}} \quad (\text{mol of } CH_4 \text{ /mole } H_2O) \tag{3.2}$$

where $\Delta n_{H,\downarrow}$ is the number of moles of gas consumed for hydrate formation at the end of experiment. $n_{H,0}$ is the number of moles of hydrates at the start of the experiment. $n_{H,t}$ is the number of moles of the hydrates at time *t*. Subscripts of *G,0* and *G,t* represent the gas phase at the start of the experiment and time *t*, respectively. *P* and *T* are the pressure and temperature in the system. *V* is the volume of gas phase in the crystallizer, *R* is the universal gas constant (82.06 cm^3atm /mol.K) and *z* is the compressibility factor calculated by Pitzer's correlation (Smith *et al.*, 2005). The rate of hydrate formation was calculated form the normalized initial hydrate formation rate (NR_t) for the first t minutes from the start of hydrate growth shown by the equation (3.3) (Veluswamy *et al.*, 2015).

$$NR_t = \frac{R_t}{V_{water}} \tag{3.3}$$

where V_{water} is the volume of water (m^3) taken in the reactor, and R_t is the rate of hydrate growth (mmol/min) calculated by fitting the average gas uptake due to hydrate growth at each experimental condition versus time for the first *t* minutes after the induction time, using the least squares method. The time period of *t* minutes that gives the best fit is selected for rate quantification based on the hydrate gas uptake profiles for all experiments.

3.5 Hydrate Dissociation Experiment

After the completion of methane hydrate formation, methane hydrates were dissociated through thermal stimulation by increasing the temperature to 25 ℃. The start of the temperature rise was considered as time zero for the hydrate dissociation experiments. The gas released from the gas hydrates was measured by the pressure transducer. The experiment was stopped when the pressure in the reactor remained constant at experimental temperature. Methane hydrates start to dissociate and continue to dissociate till the dissociation temperature of 25 ℃. Thus, at the dissociation temperature considered, all the hydrates formed was completely dissociated. The experiments were stopped when the pressure was constant at the set dissociation temperature. The number of moles of methane gas released from the hydrates during the dissociation experiment at given any time (*t*) was calculated by equation (3.4). This equation is the negative of the equation (3.1) detailed above as initially there was lower moles of gas and with the progress in dissociation number of moles of gas increases till the completion.

$$\Delta n_{H,\uparrow} = n_{H,t} - n_{H,0} = \left(\frac{PV}{zRT}\right)_{G,t} - \left(\frac{PV}{zRT}\right)_{G,0} \tag{3.4}$$

Methane recovery was calculated by equation (3.5) (Babu *et al.*, 2013; Linga *et al.*, 2009).

$$\%\text{methane recovery} = \frac{(\Delta n_{H,\uparrow})}{(\Delta n_{H,\downarrow})} \times 100 \tag{3.5}$$

$\Delta n_{H,\uparrow}$ = moles of released gas from hydrate during the hydrate dissociation at any given time.

$(\Delta n_{H,\downarrow})_{End}$ = moles of gas consumption for hydrate formation at the end of experiments.

CHAPTER 4
RESULT AND DISCUSSION

This work investigated the effects of mixed SDS with nonionic surfactants on the kinetics and morphology behavior of methane hydrate formation and dissociation. Although SDS has been reported as one of the best kinetic promoters, enhancing the rate of hydrate formation and increasing the amount of gas uptake, the amount of foam generated during the gas recovery process results in not enough memory solution for methane formation. So, the mixed surfactant has emerged as one of potentials to solve this problem. The aim of this work was to suppress the excessive amount of foam generation. The experiment was divided into two parts. Firstly, the experiment investigated the effects of mixed SDS with EO_3 and EO_5 to observe the methane hydrate formation pattern, the amount of foam reduction during the methane hydrate dissociation, and the kinetics. Secondly, the experiment involved the mixed SDS with APG to investigate the effects of carbon chain length on the foam reduction. All experiments in this work were performed with different EO_3/SDS, EO_5/SDS, and APG/SDS mass fractions, 0.0625/0.25, 0.125/0.25, and 0.25/0.25, in the quiescent system at 4 ℃ and 8 MPa, and each experiment was performed at least three times to ensure the repeatability.

First, water and single surfactant including SDS, EO_3, EO_5, and APG were used for methane hydrate formation. However, no hydrate formation was observed after 48 hr except SDS. As the surface tension of water at 4 ℃ is 69.25 mN/m, it is possible that the hydrates could not form along the interface due to higher surface tension than the solution with a surfactant, as shown in Figure 4.1. The nonionic surfactants like EO_3, EO_5, or APG, at 0.25 wt% were chosen as it is above the critical micelle concentration (CMC), lower surface tension than 0.25 wt% SDS, effective of the foam reduction, and does not affect to the hydrate formation kinetics of the mixed surfactants. In addition, the nonionic surfactants do not show any evidence of hydrate formation. It is possible that the adsorption of nonionic surfactant at the interface must be considered. Levitz (2002) reported that a nonionic surfactant adsorbs to the gas and liquid interface, but it does not provide a charge, potential, and electrostatic repulsion, which is difference from an anionic surfactant like SDS. According to Pandey *et al*.

(2018) works, they reported that 0.25 wt% SDS did not only enhance the kinetics of hydrate formation but also was the effective concentration for the foam formation during hydrate dissociation. So, 0.25 wt% SDS was also used in this work.
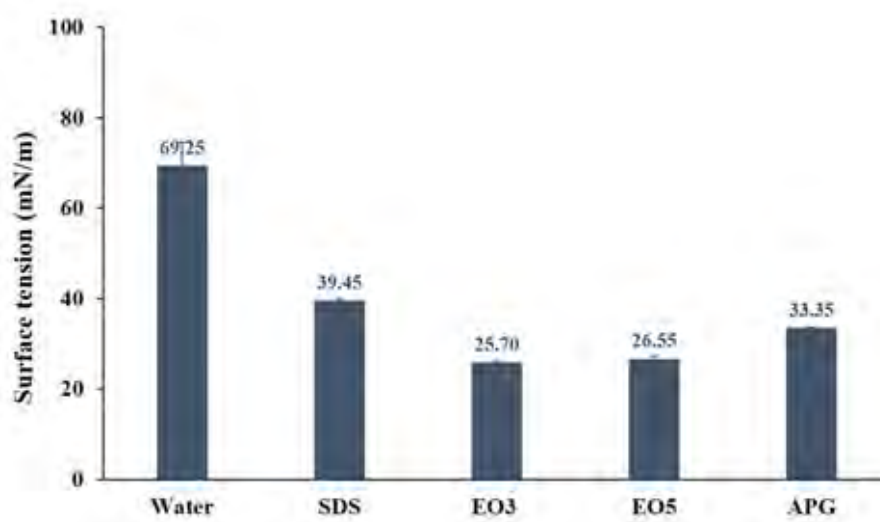
Figure 4.1 Surface tension of water, SDS, EO₃, EO₅, and APG at 0.25 wt%, at 4 ℃.

Figure 4.2 shows the gas uptake and temperature profiles during methane hydrate formation in the presence of 0.25 wt% SDS. The results show that, at 3.92 min, the gas uptake in the system gradually increases. Around 5 hr, the gas uptake is stable at 0.1402 moles of gas/mole of water, and the temperature is back to 4 ℃ as the start of the experiment, which means methane hydrate formation completes. During the methane hydrate formation, the gas uptake in the system increases, which is referred to the pressure drops in the system. and the temperature spikes up immediately as the formation is an exothermic reaction. The time when the above phenomena is observed is called induction time. For methane hydrate formation, it is desirable to have short induction time, high methane uptake, and high rate of hydrate formation. The hydrate formation mechanism in the presence of SDS starts by the cluster of gas and water molecules as a precursor of hydrate nuclei formation. Then, hydrate nucleus grows up to a critical size, which is a stable point, after that the crystal hydrate formation is achieved. At CMC, the SDS molecule covers gas and liquid interface resulting in surface tension reduction, while SDS in bulk phase forms micelle. The micellization of SDS in the bulk phase induces the hydrate nucleation in

the system. An effective critical nuclei size is lowered by surfactant absorption, which results in the higher hydrate nucleation rate. So, methane gas easily diffuses into the solution. Moreover, a thin film of hydrates at the surface solution during the hydrate formation is not a rigid film. However, it changes to the porous film, with higher surface area, which makes gas diffuse more easily into the solution.
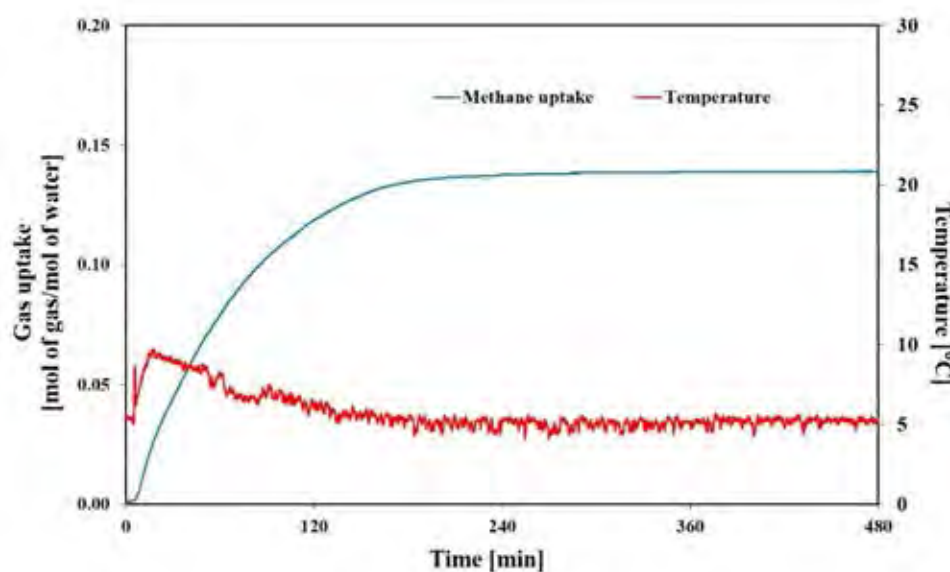
Figure 4.2 Pressure and temperature profiles during methane hydrate formation in the presence of 0.25 wt% SDS at 8 MPa and 4 ℃.

The hydrate dissociation study was performed in order to understand the hydrate decomposition and gas recovery behavior. Thermal stimulation method was used by increasing the temperature from 4 ℃ to 25 ℃, which is out of the methane hydrate stable structure or self-preservation region. Figure 4.3 presents the temperature profile of the hydrate dissociation for the methane recovery in the presence of 0.25 wt% SDS. The result shows that the temperature gradually increases and is stable at 137 min. Although the temperature of system starts at 4 ℃ and ends at 25 ℃, the temperatures at different positions are also difference. At 108 min, the temperature of the gas phase in the column (T3) takes a difference path from that of the interface (T2) and the liquid phase (T1) to reach 25 ℃. At 137 and 159 min, T1 and T2 suddenly increase to reach 25 ℃. It is clearly observed that the hydrate

structure starts to decompose at the top of the column, followed by at the bottom of the column. This is because the hydrates are denser at the interface, so the heat transfer takes longer to break the hydrates.

During the hydrate dissociation, the gas is recovered. The increase temperature results in the decomposition of hydrate structure leading to the gas coming out from the water cage. Figure 4.4 shows the pressure profile during the methane hydrate dissociation for the hydrates formation in the presence of 0.25 wt% SDS. The result shows that the pressure gradually increases due to the increasing temperature with time.
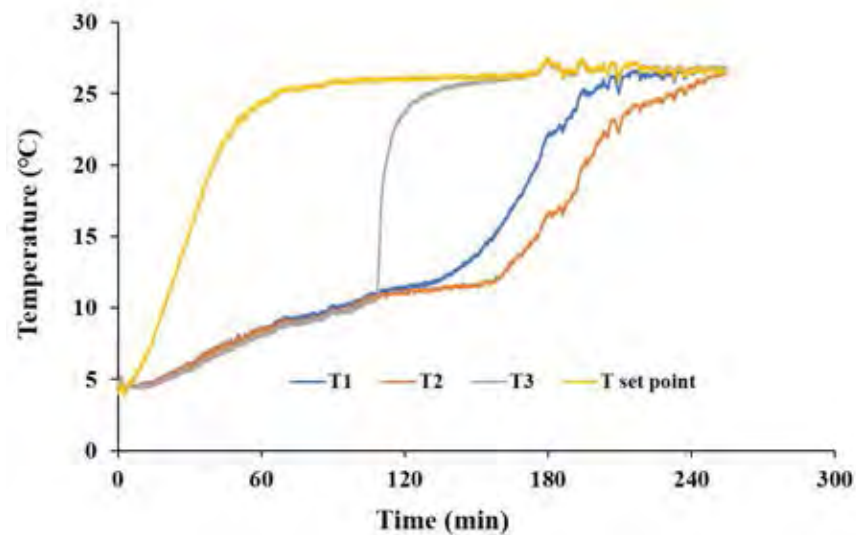
Figure 4.3 Temperature profiles during methane hydrate dissociation at different positions in the column from the hydrates formed in the presence of 0.25 wt% SDS.
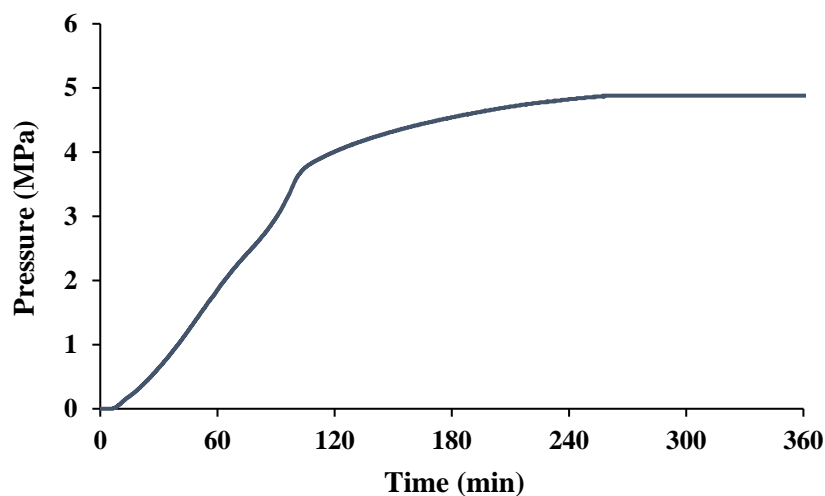
Figure 4.4 Pressure profiles during methane hydrate dissociation form the hydrates formed in the presence of 0.25 wt% SDS.

The gas storage especially methane storage via clathrate hydrate formation is now being developed for long-term and large-scale storage. Though, SDS can be used to enhance the kinetics, the morphology of hydrate formation needs to be observed for the crystallizer design. Figure 4.5 shows the series of morphology observation during methane hydrate formation in the presence of 0.25 wt% SDS at 8 MPa and 4 ℃. Figure 4.5a shows the start of the experiment. Figure 4.5b represents the hydrate nucleation at the interface of gas/liquid. This is the common phenomenon investigated for the quiescent systems as it offers a high contact area for gas and liquid phases. It is assumed that SDS aligns themselves appropriately on the gas/liquid interface resulting in the hydrate growth through capillary force at the wall of the column (Kumar *et al.*, 2015). Figure 4.5c captures the hydrates occupying along the interface of the column in 30 s. At 1 min after the nucleation, the hydrates grow in both upper and lower directions. Moreover, porous hydrates can be observed. This confirms that SDS can turn the hydrate film at the interface to a porous film, which can be increase the gas diffusion to the solution (Pandey *et al.*, 2018), as seen from Figure 4.5d. Figure 4.5e shows the hydrates occupying the entire bottom followed by the continued growth in the upper direction. Five minutes after the start of hydrate nucleation, the hydrates fully occupy the entire column, which can be observed in Figure 4.5f. The hydrates thickness in the column, as observed in Fig 4.5g. There is no significant change in the

hydrate morphology in the system after 30 min, in Figure 4.5h. However, the kinetics data were recorded until the pressure and temperature inside the column was stable.

Although SDS is known to promote the gas hydrate kinetics, it still has major limitation in making the use of SDS for long-term and large-scale storage. A large amount of foam generated especially during the hydrate dissociation becomes a real problem. In order to handle the problem, the morphology of hydrate dissociation could lead to better understanding of the behavior. Figure 4.6 shows a series of morphology observation during methane hydrate dissociation of the hydrates formed in the presence of 0.25 wt% SDS. Thermal stimulation method was used by increasing the temperature to 25 ℃. Figure 4.6a shows the start of the hydrate dissociation. After 10 min from the start, the hydrates start to dissociate from the wall of the column due to the heat transfer from the heating water, as can be seen in Figure 4.6b. Figure 4.6c shows the hydrate decomposition along the wall of the column, while the hydrate structure at the center of the column still remains unchanged. The memory solution can be observed at the bottom of column, Figure 4.6d, followed by the steady increase in the solution height and the excessive amount of foam, Figures 4.6e and 4.6f. During 5 – 8 hr from the start of hydrate dissociation, there is no significant change of the morphology in the column. Moreover, after the completion of hydrate dissociation, the undesirable foam generated remains with no reduction in the foam height even after 8 hr. This is the major obstructcle in using SDS as a kinetic promoter.
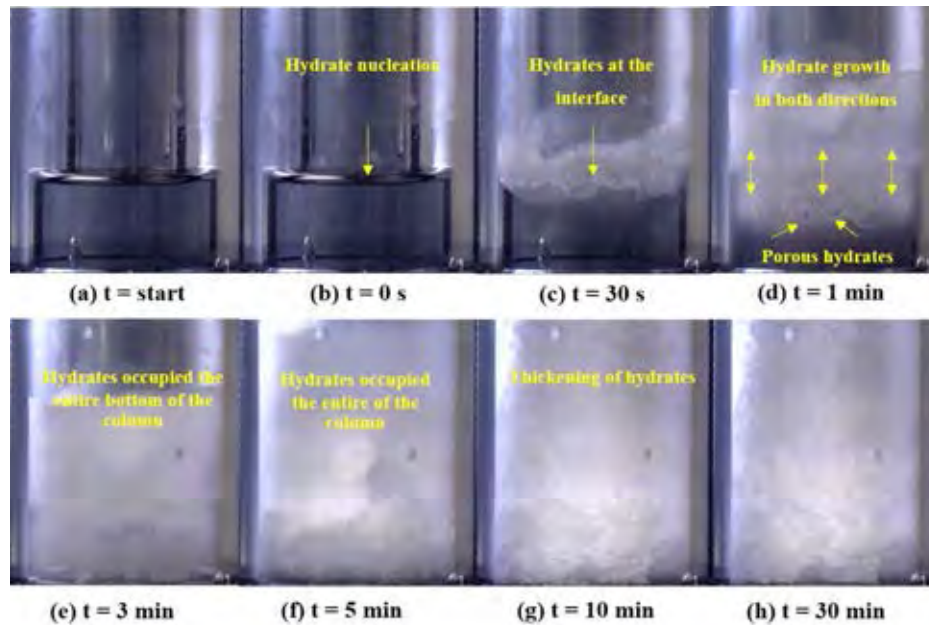
Figure 4.5 Morphology during methane hydrate formation in the presence of 0.25 wt% SDS at 8 MPa and 4 °C in the quiescent condition.
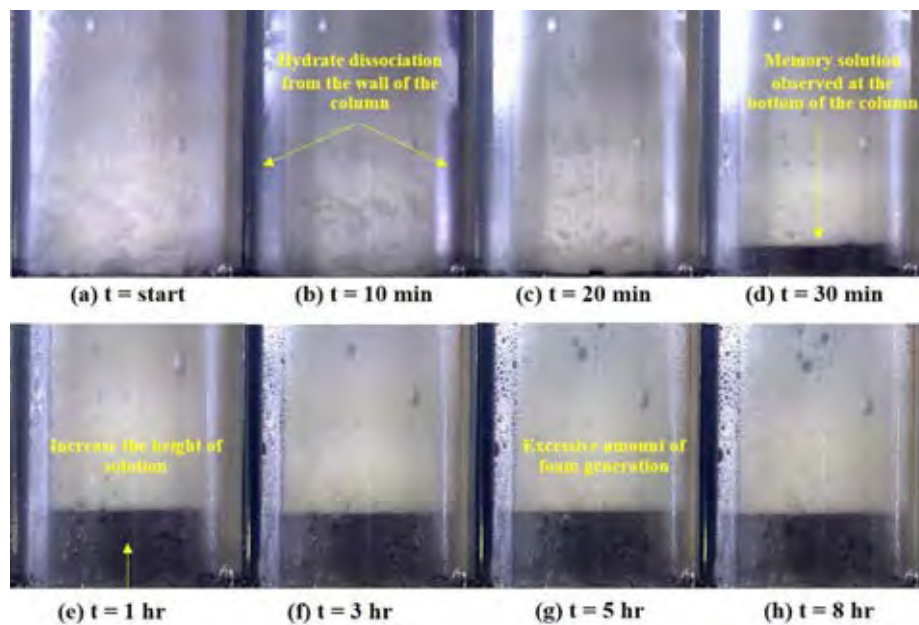
Figure 4.6 Morphology during methane hydrate dissociation from the hydrates formed in the presence of 0.25 wt% SDS at 25 °C in the quiescent condition.

To solve the foam generation during the hydrate dissociation, a defoamer was suggested as a co-promoter (Pandey *et al.*, 2018). Nonionic surfactants have emerged as a potential defoamer candidate. EO_3, EO_5, and APG are nonionic surfactants, which are used as a defoamer in commercialize technology. Although the advantage of these nonionic surfactants are inhibiting foam formation and environmentally benign, they cannot form hydrates after 48 hr. According to Ganji *et al.,* (2007), nonionic surfactants are not preferred for the hydrate experiment, so mixtures of SDS with nonionic surfactants was studied in this work to combine the advantages of SDS and nonionic surfactants by enhancing the rate of hydrate formation and gas uptake with high gas recovery and low foam formation.

4.1 Effects of EO_n/SDS

The first study in this part was performed with mixed EO_3/SDS in difference mass fractions at 8 MPa and 4 °C in the quiescent condition. Figure 4.7 shows the effects of mixed EO_3/SDS on the induction time. The result shows that in the presence of 0.25 wt% SDS, the induction time is 3.92 min, while the additional of 0.0625 wt%, 0.125 wt%, and 0.25 wt% EO_3 results in 4.11 min, 6.63 min, and 9.85 min induction time, respectively. However, the comparison on the induction time between the effects of SDS and three different mass fractions of EO_3 shows the increasing trend with the increase in the EO_3 concentration. Adding SDS results in the shortest time for hydrate formation, but the induction time gradually increases with the addition of higher concentration of EO_3. Though using nonionic surfactants as kinetic promoters in this work does not show any evidence on the hydrate formation in 48 hr, Ganji *et al*. (2007) work indicated that nonionic surfactants can induce the hydrate formation but it takes longer time to form the hydrates than using an anionic surfactant. So, in this work, it is possible that the induction time is increased when the EO_3 concentration is increased.

Figure 4.8 shows the effects of mixed EO_3/SDS on the rate of hydrate formation. The hydrate formation kinetics is considered as an important parameter for large scale storage. The normalized initial hydrate formation rate (NR_{30}) was chosen. This is the parameter referring to the rate of gas and solution converted to gas

hydrates in the system. The results show that the addition of 0.0625 wt% and 0.125 wt% EO_3 into 0.25 wt% SDS results in the same NR_{30} but adding 0.25 wt% EO_3 increases the NR_{30}. Although adding too high concentration of the nonionic surfactant results in the longer induction time, the NR_{30} increases.
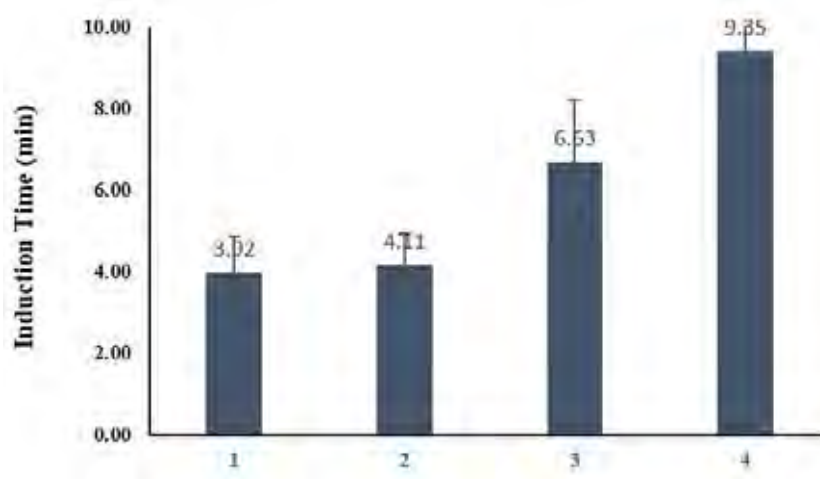
Figure 4.7 Effects of mixed EO_3/SDS in difference mass fractions on the induction time during methane hydrate formation at 8 MPa and 4 °C; (1) 0.25 wt% SDS; (2) 0.0625/0.25 wt% EO_3/SDS; (3) 0.125/0.25 wt% EO_3/SDS; (4) 0.25/0.25 wt% EO_3/SDS.
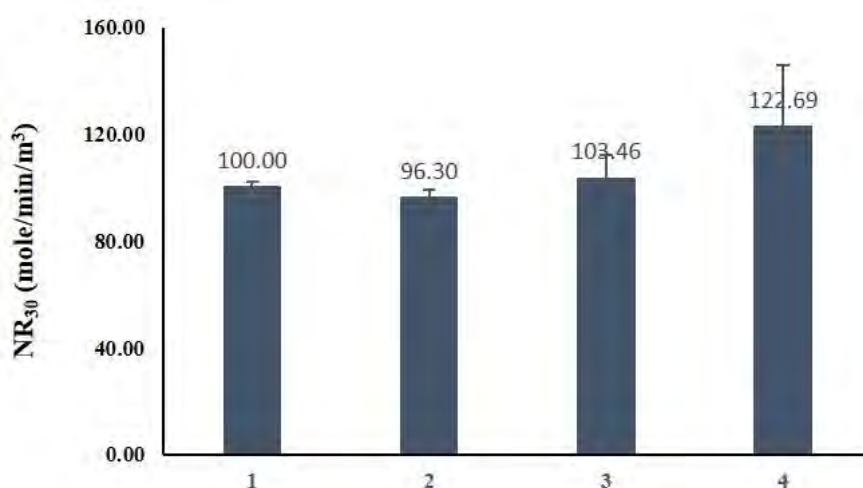
Figure 4.8 Effects of mixed EO_3/SDS in difference mass fractions on the rate of hydrate formation (NR_{30}) at 8 MPa and 4 °C; (1) 0.25 wt% SDS; (2) 0.0625/0.25 wt% EO_3/SDS; (3) 0.125/0.25 wt% EO_3/SDS; (4) 0.25/0.25 wt% EO_3/SDS.

The methane gas uptake is considered after the completion of the gas hydrate formation. Figure 4.9 shows the effects of mixed EO$_3$/SDS in difference mass fraction on the methane uptake. The methane uptake is the amount of methane gas in the column consumed and converted to methane hydrates. The result shows that there is no significant difference for the methane uptake from the system with SDS only regardless of EO$_3$ concentration. Furthermore, the difference in the uptake for using different surfactants is very minimal even during the hydrate formation, Figure 4.10.
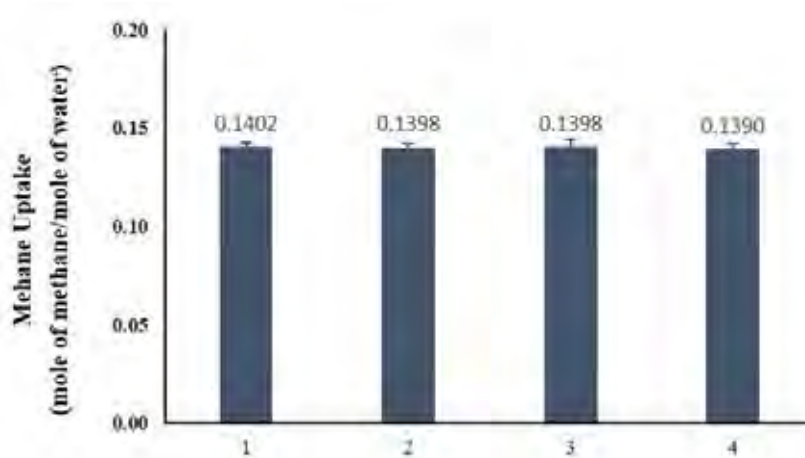
Figure 4.9 Effects of mixed EO$_3$/SDS in difference mass fractions on the methane uptake at 8 MPa and 4 ℃; (1) 0.25 wt% SDS; (2) 0.0625/0.25 wt% EO$_3$/SDS; (3) 0.125/0.25 wt% EO$_3$/SDS; (4) 0.25/0.25 wt% EO$_3$/SDS.
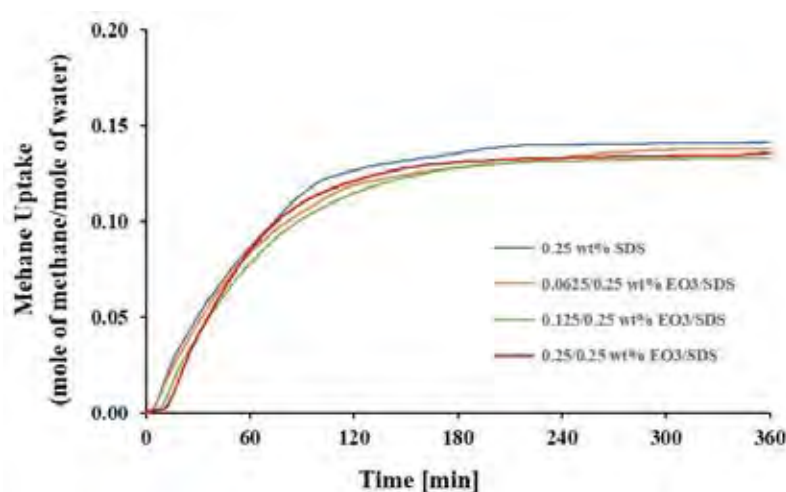
Figure 4.10 Effects of mixed EO$_3$/SDS in difference mass fractions on methane uptake with time during methane hydrate formation at 8 MPa and 4 ℃.

After the completion of hydrate formation, hydrate yield was considered. The hydrate yield is the water to hydrate conversion, which is relative with the amount of gas uptake. Therefore, the gas uptake and hydrate yield should be increased when the surface tension between gas/liquid interface is lower (Inkong *et al.*, 2019). However, the result shows that the hydrate yields of using SDS and EO_3/SDS in every mass fraction are not significantly difference. This could be due to the limitation of the water to hydrate conversion of the mixed EO_3/SDS.
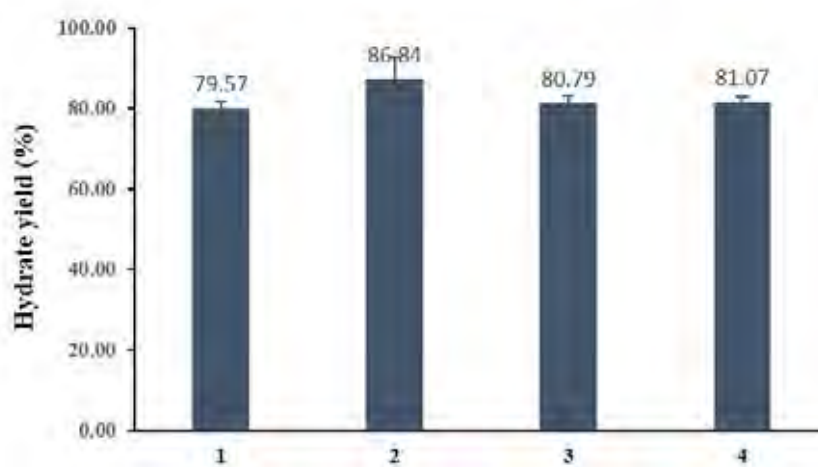
Figure 4.11 Effects of mixed EO_3/SDS in difference mass fractions on hydrate yield at 8 MPa and 4 ℃; (1) 0.25 wt% SDS; (2) 0.0625/0.25 wt% EO_3/SDS; (3) 0.125/0.25 wt% EO_3/SDS; (4) 0.25/0.25 wt% EO_3/SDS.

Furthermore, the hydrate morphology during the hydrate formation with SDS (Figure 4.12a) and EO_3/SDS (Figures 4.12b-4.12d) is shown in Figure 4.12. At the start of the experiment, the solution in the column is clearly observed along with gas phase and thermocouple, Figure 4.12b-1. Then, the hydrate nucleation presents at the gas/liquid interface at 30 s, Figure 4.12b-2. After that, the hydrates grow in both directions along with the wall of the column, Figure 4.12b-3. The hydrates occupy the entire column, and the hydrate layers can be seen at the bottom of the column. According to Inkong *et al.* (2019), the hydrate layers indicate the phenomenon of hydrate formation though capillary force along the wall of the column, and surfactant solution is transferred via porous hydrates. The thickening of hydrates can be observed, Figure 4.12b-5. There is no significant change in the morphology of hydrate

formation during 30 - 60 min. The morphology of methane hydrates formation of mixed 0.125/0.25 wt% and 0.25/0.25 wt% EO_3/SDS (Figures 4.12c, and 4.12d) shows the similar pattern with the previous experiment, starting with hydrate nucleation at the interface, hydrate growth in both directions, hydrate occupying the entire column, and thickening of hydrates. It can be concluded that the hydrate formation of mixed EO_3/SDS shows the same pattern regardless of EO_3 concentration mass fraction. Interestingly, grain like crystals are present and mushy hydrates can be observed in the downward direction during the hydrate formation of every EO_3/SDS concentration. It occurs instead of porous hydrates in the presence of 0.25 wt% SDS. Therefore, adding EO_3 with 0.25 wt% SDS results in the change in the hydrates formed in the downward direction. Moreover, in the presence of EO_3/SDS, the hydrate layers and smooth surface of hydrates formed are observed at the completion of hydrate formation.

Figure 4.13 shows the morphology during methane hydrate dissociation for the hydrates formed in the presence of SDS and mixed EO_3/SDS in difference mass fractions at 8 MPa and 4 °C. The results show similar dissociation pattern for hydrates formed at different conditions. Starting with the hydrates occupying the entire column, Figure 4.13b-1, the hydrate dissociation begins from the wall of the column at 10 min, Figure 4.13b-2. After that, the memory solution can be observed at the bottom of the column, and the excessive amount of foam can be observed, Figure 4.13b-3. The excessive amount of foam in the column remains even at 8 hr. However, the amount of foam decreases with the increase in the concentration of EO_3, as seen in Figures 4.13c-6 and 4.13d-6. Adding 0.25 wt% EO_3 with 0.25 wt% SDS seems to be effective in the foam reduction. EO_3 can reduce the foam stability, foam ability, and foam reduction depending on the amount of EO_3 added (McClure *et al.*, 2017). It is believed that when a nonionic surfactant in the solution is added, it is placed between the SDS molecules at the interface of gas/liquid resulting in the electrostatic repulsion reduction and lower the amount of foam formation (Zhu *et al.*, 2019).
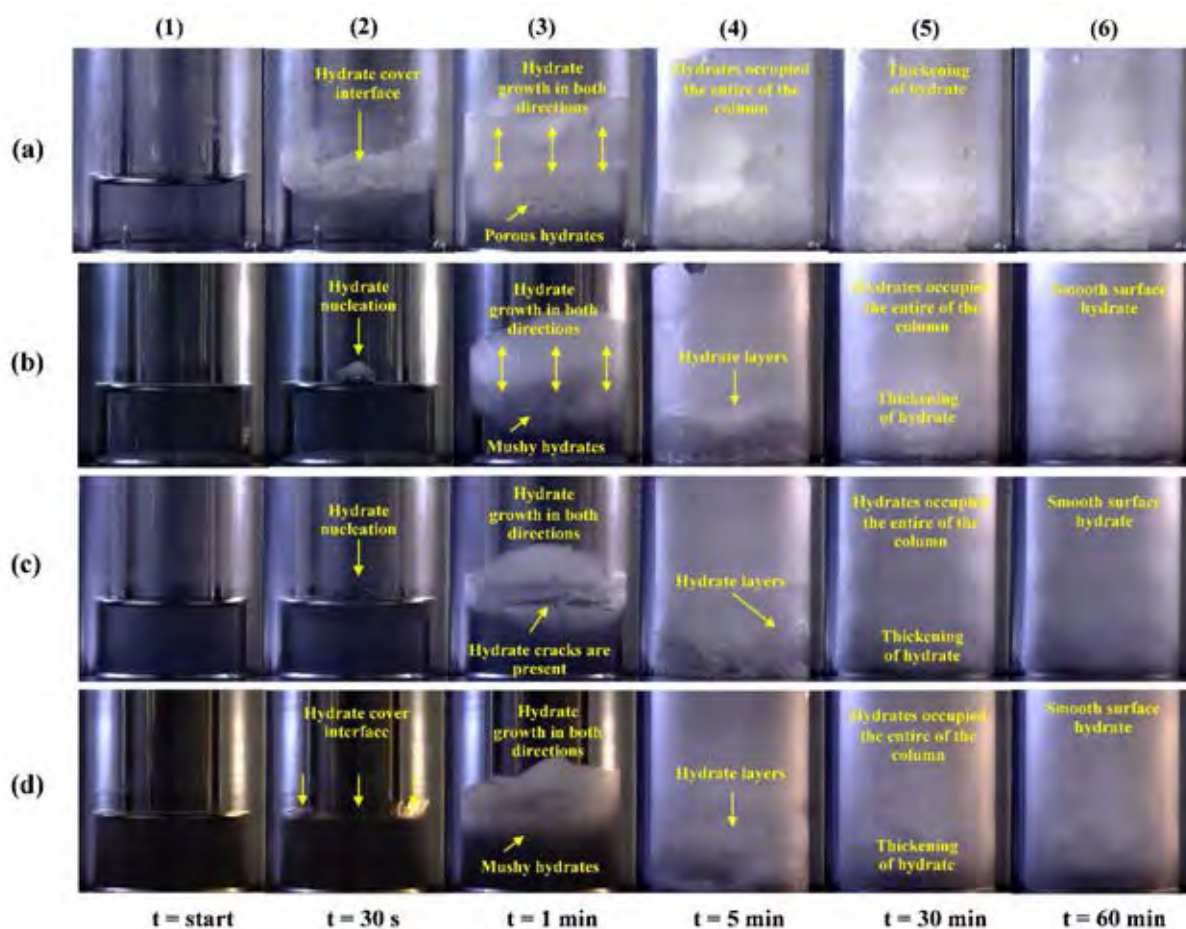
Figure 4.12 Morphology during methane hydrate formation with EO₃/SDS in difference mass fraction at 8 MPa and 4 ℃. (a) 0.25 wt% SDS; (b) 0.0625/0.25 wt% EO₃/SDS; (c) 0.125/0.25 wt% EO₃/SDS; (d) 0.25/0.25 wt% EO₃/SDS.

Although the mixed EO₃/SDS can lower the excessive amount of foam generation during the hydrate dissociation, it is not the effective for foam reduction. In order to enhance the possibility of foam reduction, EO₅ was selected as the nonionic surfactant. The more ethoxylate group means the more hydrophilic part in the chemical structure resulting in the better solubility in the solution. Therefore, the EO₅/SDS was investigated in difference mass fractions, 0.0625/0.25 wt%, 0.125/0.25 wt%, and 0.25/0.25 wt% EO₅/SDS at 8 MPa and 4 ℃ in the quiescent condition.
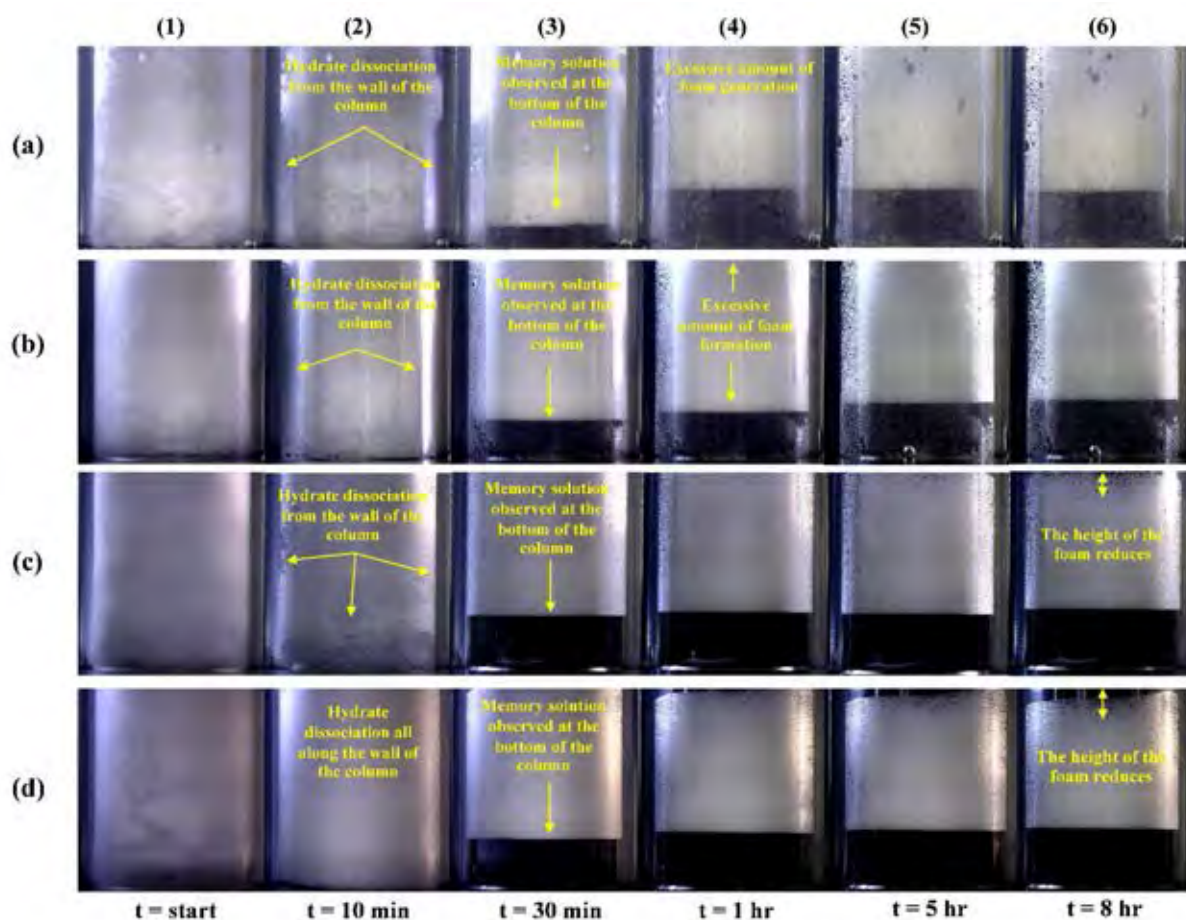
Figure 4.13 Morphology during methane hydrate dissociation from the hydrates formed in the presence of mixed EO₃/SDS in difference mass fractions at 25 ℃. (a) 0.25 wt% SDS; (b) 0.0625/0.25 wt% EO₃/SDS; (c) 0.125/0.25 wt% EO₃/SDS; (d) 0.25/0.25 wt% EO₃/SDS.

Figure 4.14 shows the morphology during methane hydrate formation in 0.25 wt% SDS, 0.0625/0.25 wt%, 0.125/0.25 wt%, and 0.25/0.25 wt% EO₅/SDS at at 8 MPa and 4 ℃. It is clear that the hydrate formation in the presence of mixed EO₅/SDS shows the commonly observed of methane hydrate formation pattern in the quiescent condition. Starting with the hydrate nucleation at the gas/liquid interface, hydrates continue to grow in both directions, and the hydrates occupy the entire column before the thickening of hydrates is observed. The similar formation behavior can be observed regardless of EO₅ concentration, Figures 4.14b - 4.14d. Interestingly, during the hydrate growth in both directions, the hydrate cracks are present for every

EO$_5$/SDS concentration. It could be become the hydrate density in the downward direction is higher than the upward direction resulting in the hydrate cracks. However, the completion of hydrate formed with EO$_5$/SDS is difference from 0.25 wt% SDS. For example, at the bottom, the hydrates are not as dense as that with SDS. It is possible that, after the hydrate cracks are present, the hydrates do not grow in the downward direction but in the upward direction. Moreover, the porous hydrates can be seen similar to the case with 0.25 wt% SDS.

Moreover, the morphology of methane hydrate dissociation for hydrates formed in the presence of SDS and mixed EO$_5$/SDS can be observed, Figure 4.15. Figure 4.15b-1 presents the start of the hydrate dissociation of hydrates formed in 0.0625/0.25 wt% EO$_5$/SDS. The decomposition begins from the wall of the column at 10 min from the start, Figure 4.15b-2. After that, the hydrates decompose along the entire wall column, while those at the center of the column remain, Figure 4.15b-3. Memory solution and excess foam formation can be observed, Figure 4.15b-4. During 1 − 8 hr from the start, there is no significant change on the foam height in the column, Figures 4.15b-5 and 4.15b-6. The decomposition of hydrates formed with 0.125/0.25 wt% EO$_5$/SDS has similar pattern as Figure 4.15b with 0.0625/0.25 wt% EO$_5$/SDS including no change in the foam height. However, the hydrates formed with 0.25/0.25 wt% EO$_5$/SDS decompose similarly but the amount of foam generated is difference. Figure 4.15d-2 shows the decomposition begins at the wall of the column, followed by memory solution at the bottom of the column, Figure 4.15d-3. The reduction of foam height can be observed in 1 hr, and the generated foam changes into fine and smaller bubble sizes. Moreover, the foam height gradually decreases from 1 − 8 hr, Figure 4.15d-4, 4.15d-5, and 4.15d-6. It is possible that the more ethoxylate group in the chemical structure resulting in EO$_5$ dispersed well in the solution and placed between the SDS molecules. Therefore, electrostatic repulsion in the solution reduces with foam ability and foam stability. However, 0.25/0.25 wt% EO$_5$/SDS seems to be the effective mass fractions among the standard EO$_5$/SDS. It is possible that EO$_5$ concentration must be the high enough to show the foam reduction.
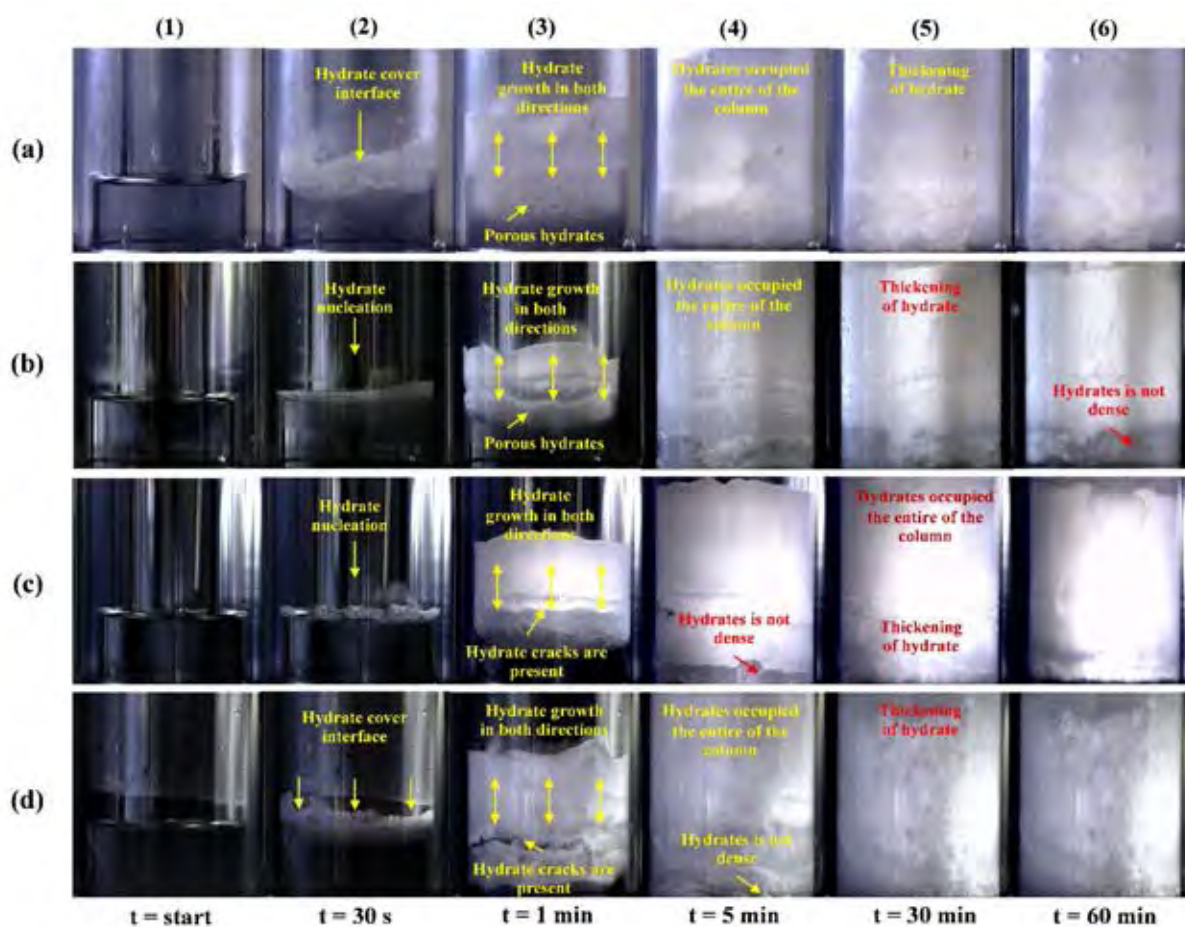
Figure 4.14 Morphology during methane hydrate formation with mixed EO_5/SDS in difference mass fraction at 8 MPa and 4 °C. (a) 0.25 wt% SDS; (b) 0.0625/0.25 wt% EO_3/SDS; (c) 0.125/0.25 wt% EO_3/SDS; (d) 0.25/0.25 wt% EO_3/SDS.

Moreover, the methane hydrate kinetics of mixed EO_5/SDS was investigated. The experiment was performed at 8 MPa and 4 °C in the quiescent condition. Figure 4.16 was present the effects of mixed EO_5/SDS in difference mass fractions on the induction. The results show that the addition of 0.0625 wt%, 0.125 wt%, and 0.25 wt% EO_5 results in 6.67 min, 1.72 min, and 4.11 min induction time, respectively. The comparison of induction times indicates that there is no predicable trend with the addition of EO_5. This result presents the stochastic phenomenon of methane hydrate formation in the presence of mixed EO_5/SDS.
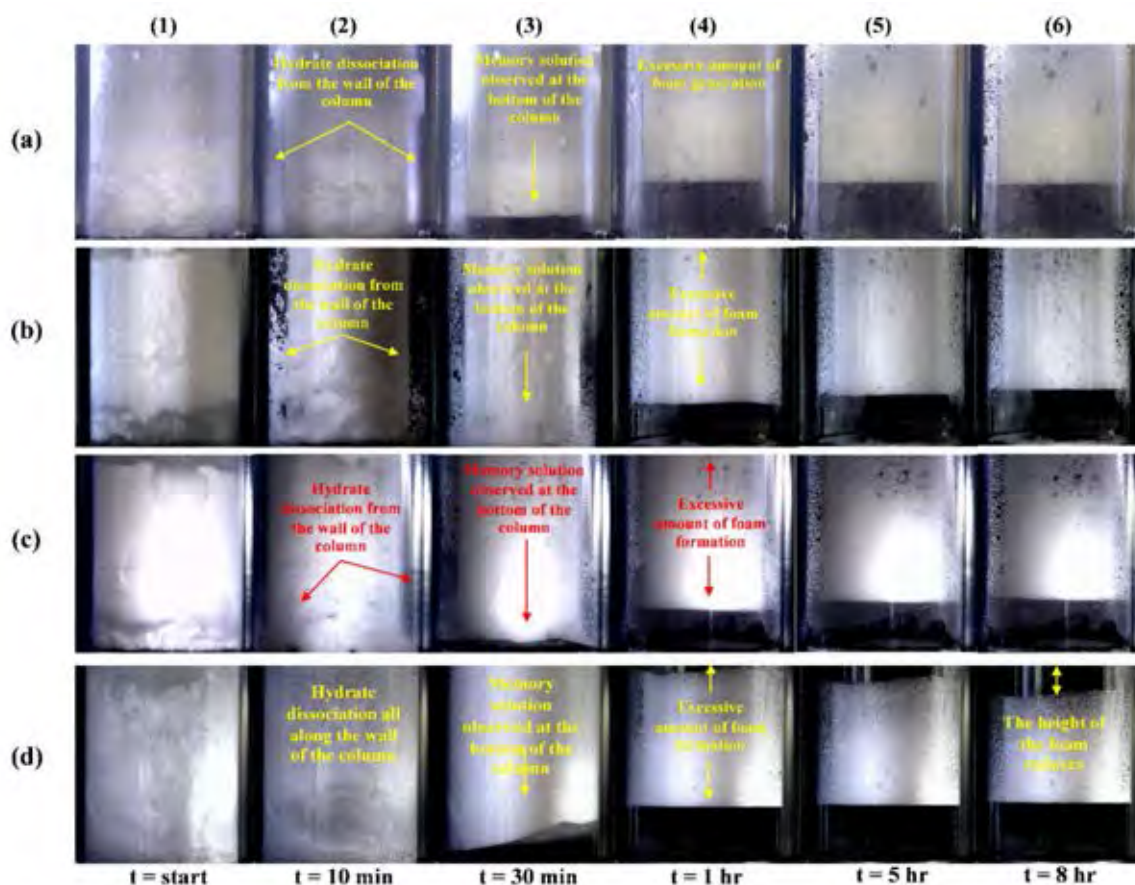
Figure 4.15 Morphology during methane hydrate dissociation from the hydrates formed in the presence of mixed EO5/SDS in difference mass fractions at 25 ℃. (a) 0.25 wt% SDS; (b) 0.0625/0.25 wt% EO3/SDS; (c) 0.125/0.25 wt% EO3/SDS; (d) 0.25/0.25 wt% EO3/SDS.

Figure 4.17 shows the effect of mixed EO5/SDS in difference mass fractions on the rate of hydrate formation. The results show that the addition of 0.0625 wt%, 0.125 wt%, and 0.25 wt% EO5 result in 91.94 mole/min/m^3, 100.06 mole/min/m^3, and 86.85 mole/min/m^3, respectively. This result presents the unpredictable trend with EO5 concentration. Figure 4.18 indicates that, in the presence of mixed EO5/SDS, there is no significant difference for the methane uptake from the system with SDS only. Furthermore, the difference in the uptake with different EO5 concentrations is very minimal even during the hydrate formation.
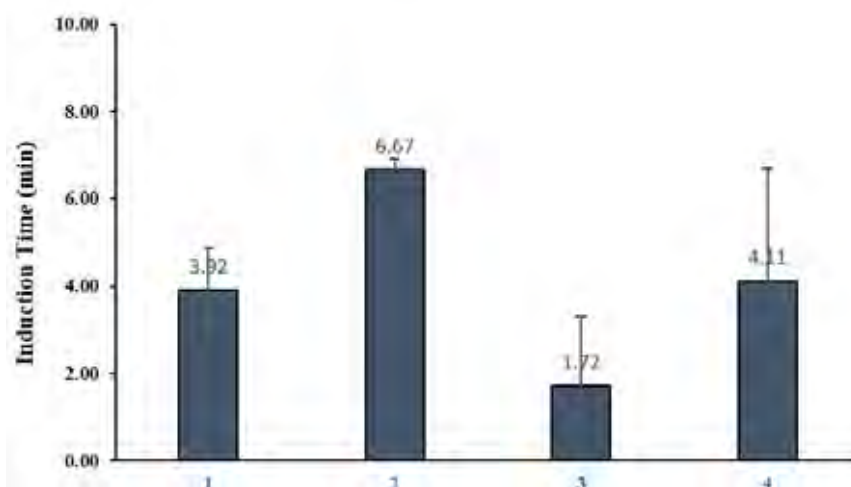
Figure 4.16 Effects of mixed EO_5/SDS in difference mass fractions on the induction time during methane hydrate formation at 8 MPa and 4 °C; (1) 0.25 wt% SDS; (2) 0.0625/0.25 wt% EO_5/SDS; (3) 0.125/0.25 wt% EO_5/SDS; (4) 0.25/0.25 wt% EO_5/SDS.
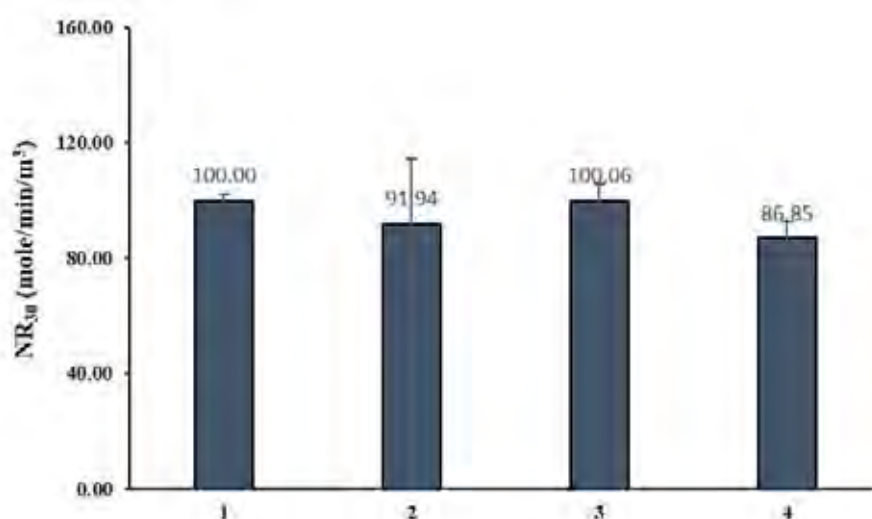
Figure 4.17 Effects of mixed EO_5/SDS in difference mass fractions on the rate of hydrate formation (NR_{30}) at 8 MPa and 4 °C; (1) 0.25 wt% SDS; (2) 0.0625/0.25 wt% EO_5/SDS; (3) 0.125/0.25 wt% EO_5/SDS; (4) 0.25/0.25 wt% EO_5/SDS.

Figure 4.19 shows effects of mixed EO_5/SDS in difference mass fractions on hydrate yield at 8 MPa and 4 °C. The result indicates that the addition of 0.0625 wt%, 0.125 wt%, and 0.25 wt% EO_5 results in 81.43%, 81.69%, and 80.18% yield,

respectively. There is no significant difference compared to the presence of only 0.25 wt% SDS. This could be the hydrate formation in the presence of mixed EO$_5$/SDS reaches the optimum water to hydrate conversion.

Figure 4.18 Effects of mixed EO$_5$/SDS in difference mass fractions on the methane uptake at 8 MPa and 4 ℃; (1) 0.25 wt% SDS; (2) 0.0625/0.25 wt% EO$_5$/SDS; (3) 0.125/0.25 wt% EO$_5$/SDS; (4) 0.25/0.25 wt% EO$_5$/SDS.
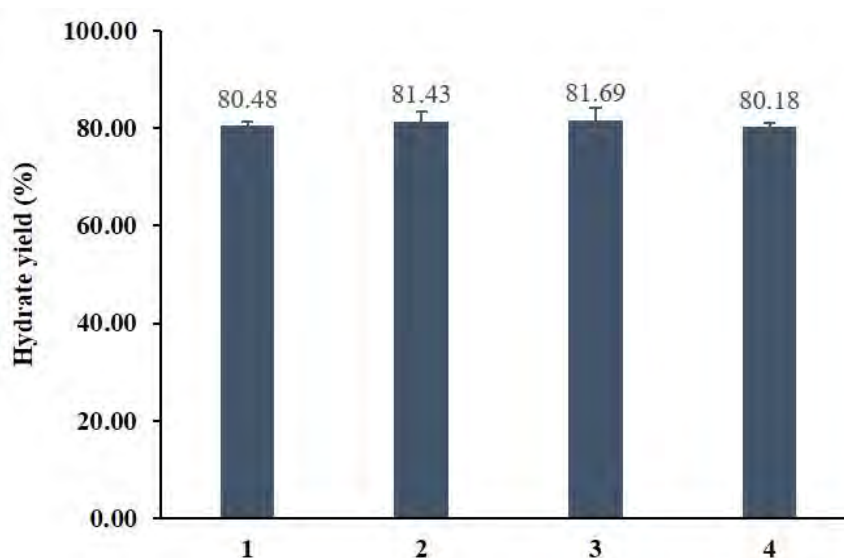
Figure 4.19 Effects of mixed EO$_5$/SDS in difference mass fractions on hydrate yield at 8 MPa and 4 ℃; (1) 0.25 wt% SDS; (2) 0.0625/0.25 wt% EO$_5$/SDS; (3) 0.125/0.25 wt% EO$_5$/SDS; (4) 0.25/0.25 wt% EO$_5$/SDS.

4.2 Effects of APG/SDS

The experiment in this part was performed using mixed APG/SDS in difference mass fractions at 8 MPa and 4 ℃ in the quiescent condition. The objective of this part is to study the methane hydrate formation kinetics and foam reduction during the dissociation of mixed APG/SDS. Figure 4.20 shows the effects of mixed APG/SDS in difference mass fractions on the induction time. The result shows that the addition of 0.0625 wt%, 0.125 wt%, and 0.25 wt% APG results in 11.00 min, 18.92 min, and 33.11 min induction time, respectively. However, the comparison on the induction time with SDS and the three different mass fractions of APG, shows an increasing trend with the increase in the APG concentration. With the addition of APG, the induction time increases up to ten times higher than the addition of SDS alone. It is possible that the higher the carbon chain length in APG, the longer the induction time.

Figure 4.21 shows the effects of mixed APG/SDS in difference mass fractions on the rate of hydrate formation. The result shows that the increase in the APG concentration results in the low hydrate formation rate except 0.0625 wt% APG. In the presence of APG mixed with SDS, not only is the induction time higher, but also the rate of hydrate formation is lower. As APG is a viscous surfactant, it is possible that the addition of APG increases the mass transfer resistance between gas/liquid interface (Bhattacharjee *et al.*, 2020). Moreover, the larger the hydrophobic part in the APG structure, the higher the APG concentration is added resulting in the difficulty in the solubility of APG in the solution. So, the induction time is higher when the APG concentration increases.

Figure 4.22 presents the effects of mixed APG/SDS in difference mass fractions on the methane uptake at 8 MPa and 4 ℃. It is interesting to observe that the addition of mixed APG/SDS results in the similar methane uptake during the hydrate formation compared with 0.25 wt% SDS, albeit low hydrate formation rate and high induction time. Moreover, the hydrate yield is considered, as shown in Figure 4.23. In the presence of every mass fraction of mixed APG/SDS, the hydrate yield is similar to 0.25 wt% SDS alone.

Figure 4.20 Effects of mixed APG/SDS in difference mass fractions on the induction time during methane hydrate formation at 8 MPa and 4 ℃; (1) 0.25 wt% SDS; (2) 0.0625/0.25 wt% APG/SDS; (3) 0.125/0.25 wt% APG/SDS; (4) 0.25/0.25 wt% APG/SDS.
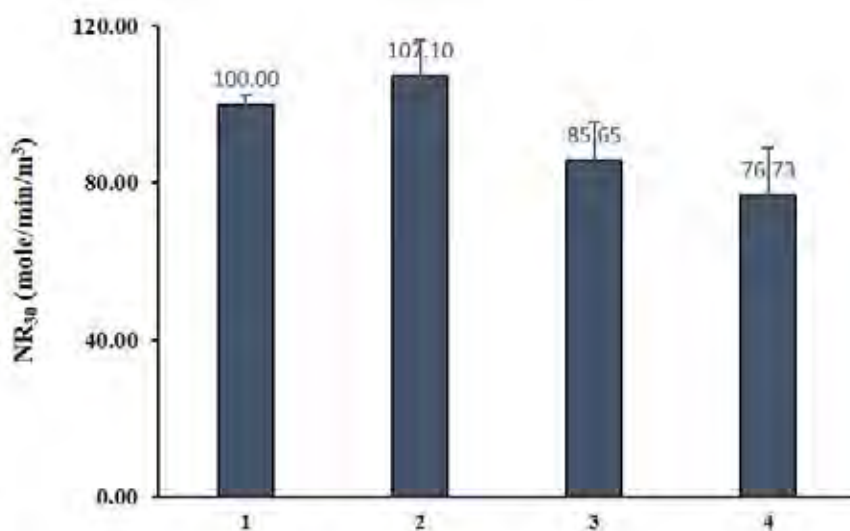
Figure 4.21 Effects of mixed APG/SDS in difference mass fractions on the rate of hydrate formation (NR_{30}) at 8 MPa and 4 ℃; (1) 0.25 wt% SDS; (2) 0.0625/0.25 wt% APG/SDS; (3) 0.125/0.25 wt% APG/SDS; (4) 0.25/0.25 wt% APG/SDS.
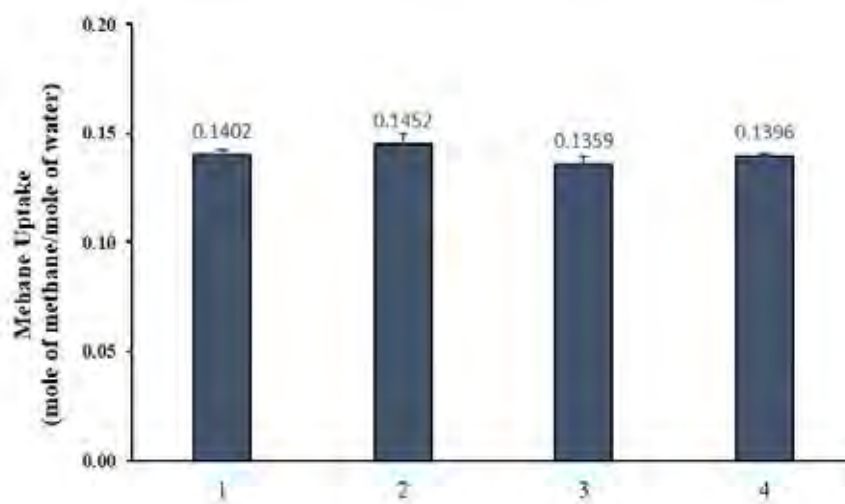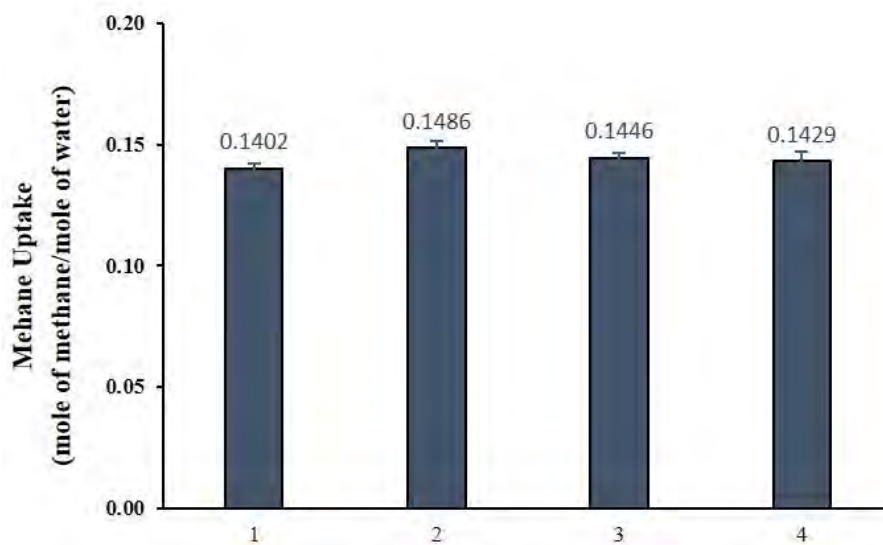
Figure 4.22 Effects of mixed APG/SDS in difference mass fractions on the methane uptake at 8 MPa and 4 ℃; (1) 0.25 wt% SDS; (2) 0.0625/0.25 wt% APG/SDS; (3) 0.125/0.25 wt% APG/SDS; (4) 0.25/0.25 wt% APG/SDS.

Furthermore, the hydrate morphology during the hydrate formation with APG/SDS is shown in Figure 4.24. The experiment was performed with difference mass fractions of APG/SDS at 8 MPa and 4 °C in the quiescent condition. For 0.0625/0.25 wt% APG/SDS, at the start of the experiment, the solution in the column is clearly observed along with the gas phase and thermocouple, Figure 4.24b-1, followed by the hydrate nucleation at the gas/liquid interface, Figure 4.24b-2. Then, the hydrates continue to grow in both directions, Figure 4.24b-3. However, its growth from the right side of the column is faster than on the left side. After that, the hydrates almost occupy the entire column at 5 min from the start, Figure 4.24b-4. Thickening hydrates can be observed at 30 min from the start, Figure 4.24b-5. The hydrate formation with all mixed APG/SDS shows the similar pattern, in Figures 4.24c and 4.24d. Interestingly, adding APG shows the mushy hydrates instead of porous hydrates in the downward direction during hydrate formation compared with 0.25 wt% SDS. Moreover, vein-like structures can be seen on the column wall with APG/SDS, which is difference from SDS.
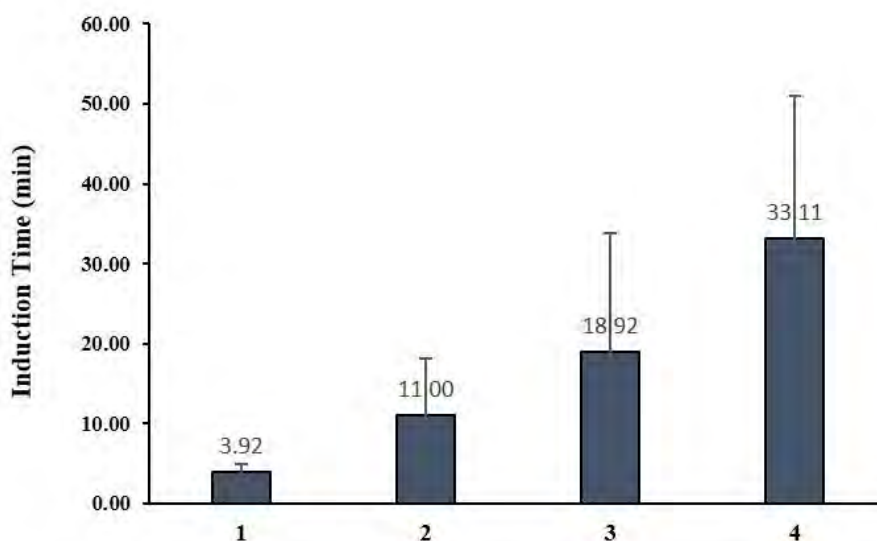
Figure 4.23 Effects of mixed APG/SDS in difference mass fractions on hydrate yield at 8 MPa and 4 ℃; (1) 0.25 wt% SDS; (2) 0.0625/0.25 wt% APG/SDS; (3) 0.125/0.25 wt% APG/SDS; (4) 0.25/0.25 wt% APG/SDS.

Moreover, the morphology of methane hydrate dissociation from the hydrates formed in the presence of mixed APG/SDS was observed. The addition 0.0625 wt% of APG shows the hydrate decomposition begins from the wall of the column at 10 min from the start, Figure 4.25b-2. After that memory solution and excess foam formation can be observed, Figure 4.25b-3. Figure 4.25b-4, during 1 – 8 hr from the start, there is no significant change on the foam height in the column, Figures 4.25b-4, 4.25b-5, and 4.25b-6. The decomposition of hydrate formed with 0.125/0.25 wt% APG/SDS has similar pattern as Figure 4.25b with 0.0625/0.25 wt% APG/SDS including no change for the foam high. However, the hydrates formed with 0.25/0.25 wt% APG/SDS decompose differently. The hydrate starts to decompose along the entire wall column, while at the center of the column remains, Figure 4.25d-2. Followed by memory solution observed at the bottom of the column, Figure 4.25d-3, Figure 4.25d-4, the reduction of foam height can be observed in 1 hr. Moreover, the foam height gradually decreases from 1 – 8 hr, Figure 4.25d-5 and 4.25d-6.
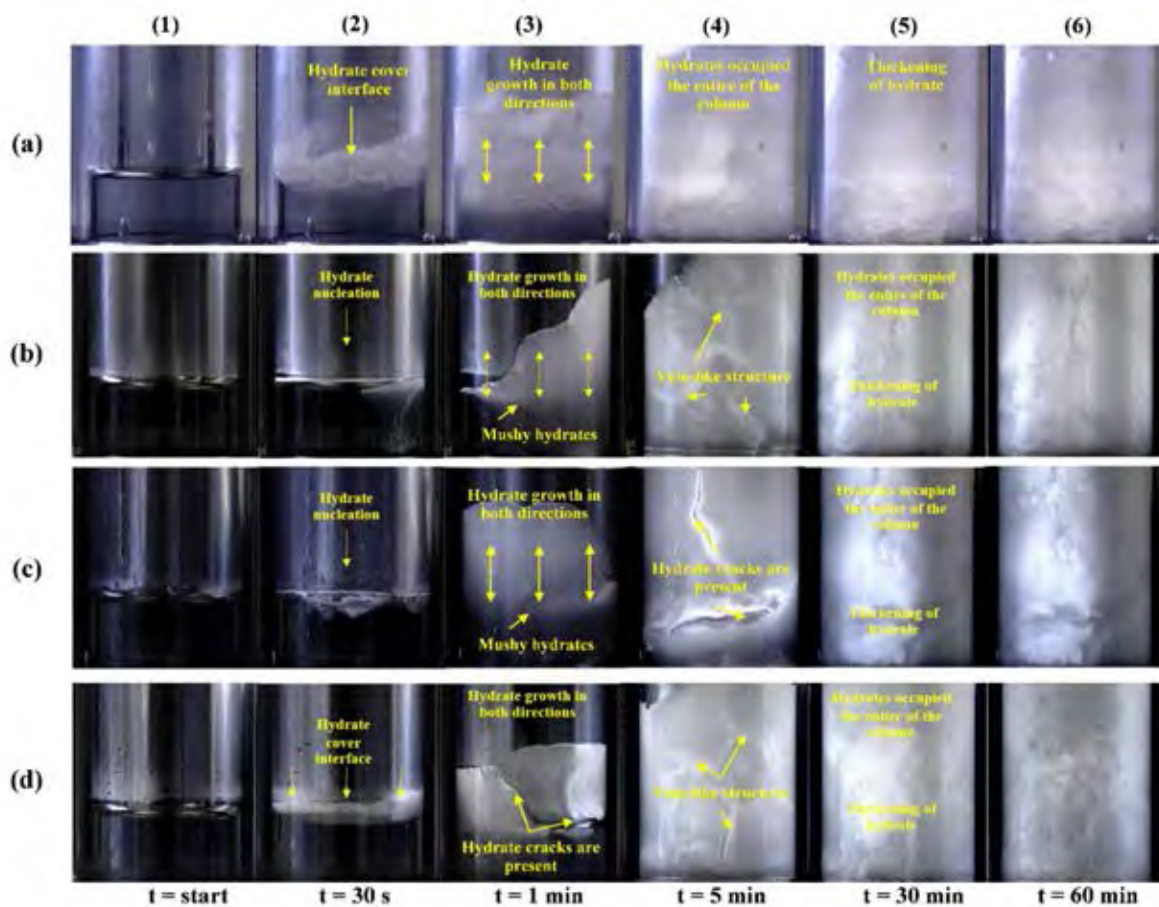
Figure 4.24 Morphology during methane hydrate formation of mixed APG/SDS in difference mass fractions at 8 MPa and 4 °C. (a) 0.25 wt% SDS (b) 0.0625/0.25 wt% APG/SDS; (c) 0.125/0.25 wt% APG/SDS; (c) 0.25/0.25 wt% APG/SDS.

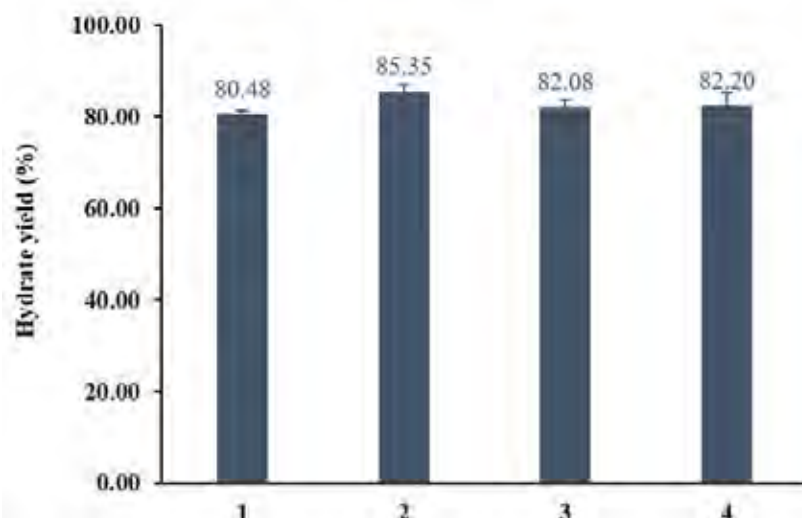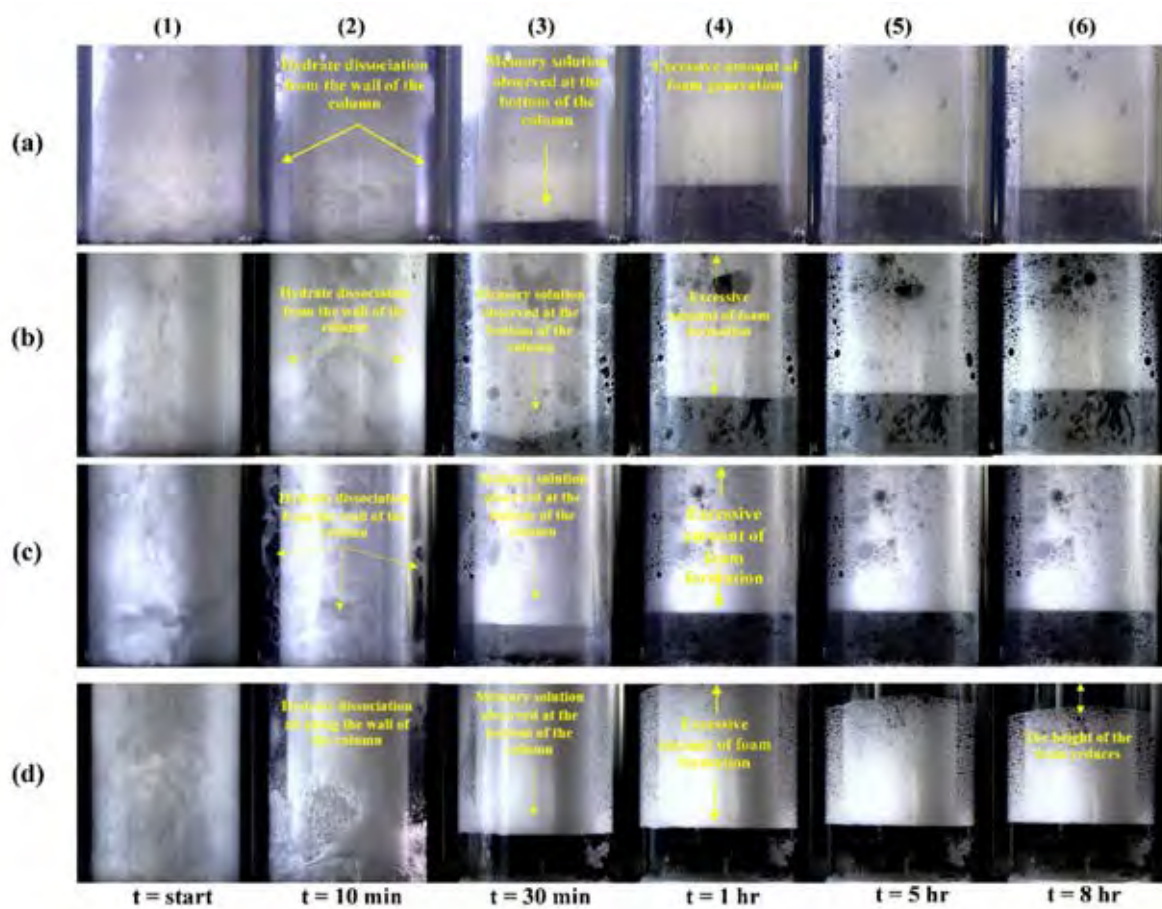**Figure 4.25** Morphology during methane hydrate dissociation from the hydrates formed in the presence of mixed APG/SDS in difference mass fraction at 25 ℃. (a) 0.25 wt% SDS (b) 0.0625/0.25 wt% APG/SDS; (c) 0.125/0.25 wt% APG/SDS; (c) 0.25/0.25 wt% APG/SDS.

4.3 Comparison among Investigated Surfactants

Table 4.1 Hydrate formation experimental conditions at 8 MPa and 4 °C

Composition	Concentration (wt%)	No.	Induction Time (min)	Gas Uptake (mole of gas/ mole of water)	NR_{30} (mole of gas/min/m^3 of water)
Water		1	NH	-	-
		2	NH	-	-
		3	NH	-	-
EO_3	0.25	1	NH	-	-
		2	NH	-	-
		3	NH	-	-
EO_5	0.25	1	NH	-	-
		2	NH	-	-
		3	NH	-	-
APG	0.25	1	NH	-	-
		2	NH	-	-
		3	NH	-	-
SDS	0.25	1	3.42	0.1417	101.48
		2	5.33	0.1396	92.59
		3	4.42	0.1387	98.52
EO_3/SDS	0.0625/0.25	1	1.83	0.1412	98.52
		2	3.00	0.1383	94.07
		3	7.50	0.1608	136.85
EO_3/SDS	0.125/0.25	1	8.40	0.1348	93.33
		2	6.10	0.1428	106.67
		3	5.40	0.1419	110.37
EO_3/SDS	0.25/0.25	1	1.30	0.1378	98.15
		2	8.40	0.1411	106.48
		3	10.30	0.1368	138.89

52

CU iThesis 6171001063 thesis / recv: 15072563 16:53:42 / seg: 17

Table 4.1 (Continued)

Composition	Concentration (wt%)	No.	Induction Time (min)	Gas Uptake (mole of gas/ mole of water)	NR_{30} (mole of gas/min/m^3 of water)
EO$_5$/SDS	0.0625/0.25	1	6.83	0.1400	107.18
		2	6.5	0.1485	76.11
		3	6.84	0.1470	91.94
EO$_5$/SDS	0.125/0.25	1	0.17	0.1404	99.26
		2	3.33	0.1336	94.81
		3	1.67	0.1337	106.11
EO$_5$/SDS	0.25/0.25	1	1.67	0.1383	90.56
		2	6.83	0.1398	80.00
		3	3.83	0.1406	90.00
SDS/APG	0.0625/0.25	1	15.17	0.1462	96.67
		2	15.17	0.1514	114.26
		3	2.67	0.1479	110.37
SDS/APG	0.125/0.25	1	8.33	0.1404	99.26
		2	29.5	0.1336	94.81
		3	18.92	0.1337	106.11
SDS/APG	0.25/0.25	1	11.67	0.1383	90.56
		2	55.5	0.1398	80.14
		3	32.17	0.1406	89.86

NH: no hydrate formation was observed for 48 hr.

Table 4.1 comprehensively summarizes the experimental observation for all experiments conducted with single surfactant and mixed EO$_3$/SDS, EO$_5$/SDS, and APG/SDS with difference concentrations. This table also includes the induction time, the gas uptake, and the rate of hydrate formation. Pure water and single surfactant including EO$_3$, EO$_5$, and APG do not show any evidence on hydrate formation for 48 hr. However, SDS play an important role on the hydrate formation as a kinetic promoter. The comparison on induction time shows a slight increase in the induction time when EO$_3$ or EO$_5$ is added, while the addition of APG shows the highest induction time from all experiments. For the methane uptake, the results show no significant difference between the addition of EO$_3$/SDS, EO$_5$/SDS, or APG/SDS. It is confirmed that the addition of nonionic surfactants does not affect the methane

hydrate kinetics in the presence of SDS. Moreover, the rate of hydrate formation is similar to the induction time, which is not significantly different with the addition of mixed EO_3/SDS or EO_5/SDS, while, with APG/SDS, the lowest rate of hydrate formation is observed.

Figure 4.26 magnifies the comparison of methane hydrate dissociation from the hydrates formed with SDS, EO_3/SDS, EO_5/SDS, and APG/SDS at 0.25/0.25 wt%, which is the effective concentration for foam reduction. The results show that, in the presence of only 0.25 wt% SDS, a large amount of foam generated during hydrate dissociation is observed, Figure 4.26a. Using mixed EO_3/SDS shows the foam reduction and the foam generated changed into fine and smaller bubble sizes and clear memory solution, Figure 4.26b. Interestingly, mixed 0.25/0.25 wt% EO_5/SDS seems to be effective in decreasing the foam height among all surfactants, and higher memory solution can be observed after 8 hr. Moreover, the foam generated is fine with small bubble sizes and clear memory solution, Figure 4.26c. Figure 4.26d shows that using 0.25/0.25 wt% APG/SDS results in the similar foam reduction as that with 0.25/0.25 wt% EO_5/SDS at 8 hr but the foam bubbles remain in the memory solution resulting in the unclear memory solution.

Figure 4.27 shows the comparison of methane hydrate formation kinetics of 0.25 wt% SDS, 0.25/0.25 wt% EO_3/SDS, 0.25/0.25 wt% EO_5/SDS, and 0.25/0.25 wt% APG/SDS. The results show no significant difference in the induction time with SDS and EO_5/SDS, while it slightly increase with EO_3/SDS. For APG/SDS, the induction time is increased up to ten times compared to only SDS. The rate of hydrate formation with EO_3/SDS is the highest, while the rate gradually decreases with EO_5 and APG. However, the methane uptake stays relatively the same for all experiments.
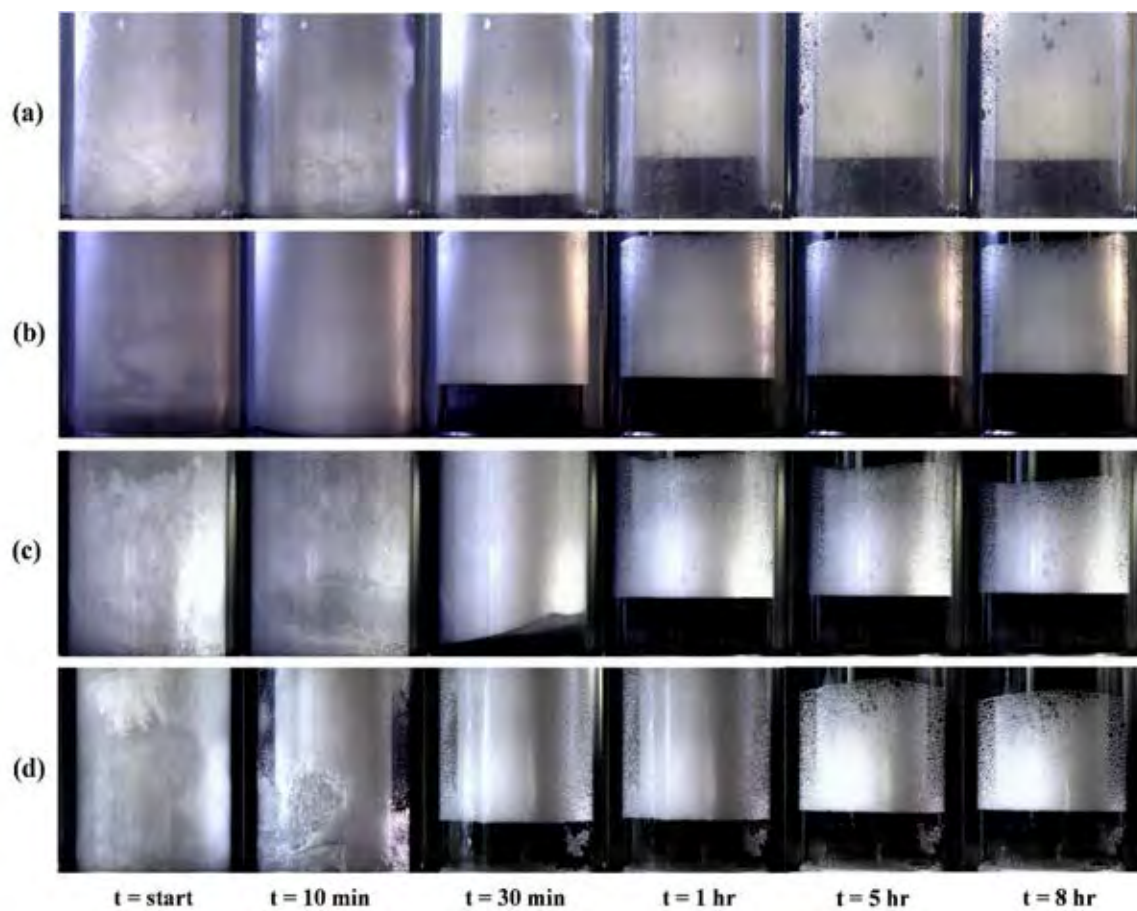
Figure 4.26 Comparison of methane hydrate dissociation from hydrates formed in the presence of (a) 0.25 wt% SDS; (b) 0.25/0.25 wt% EO₃/SDS; (c) 0.25/0.25 wt% EO₅/SDS; (d) 0.25/0.25 wt% APG/SDS at 25 °C in the quiescent condition.
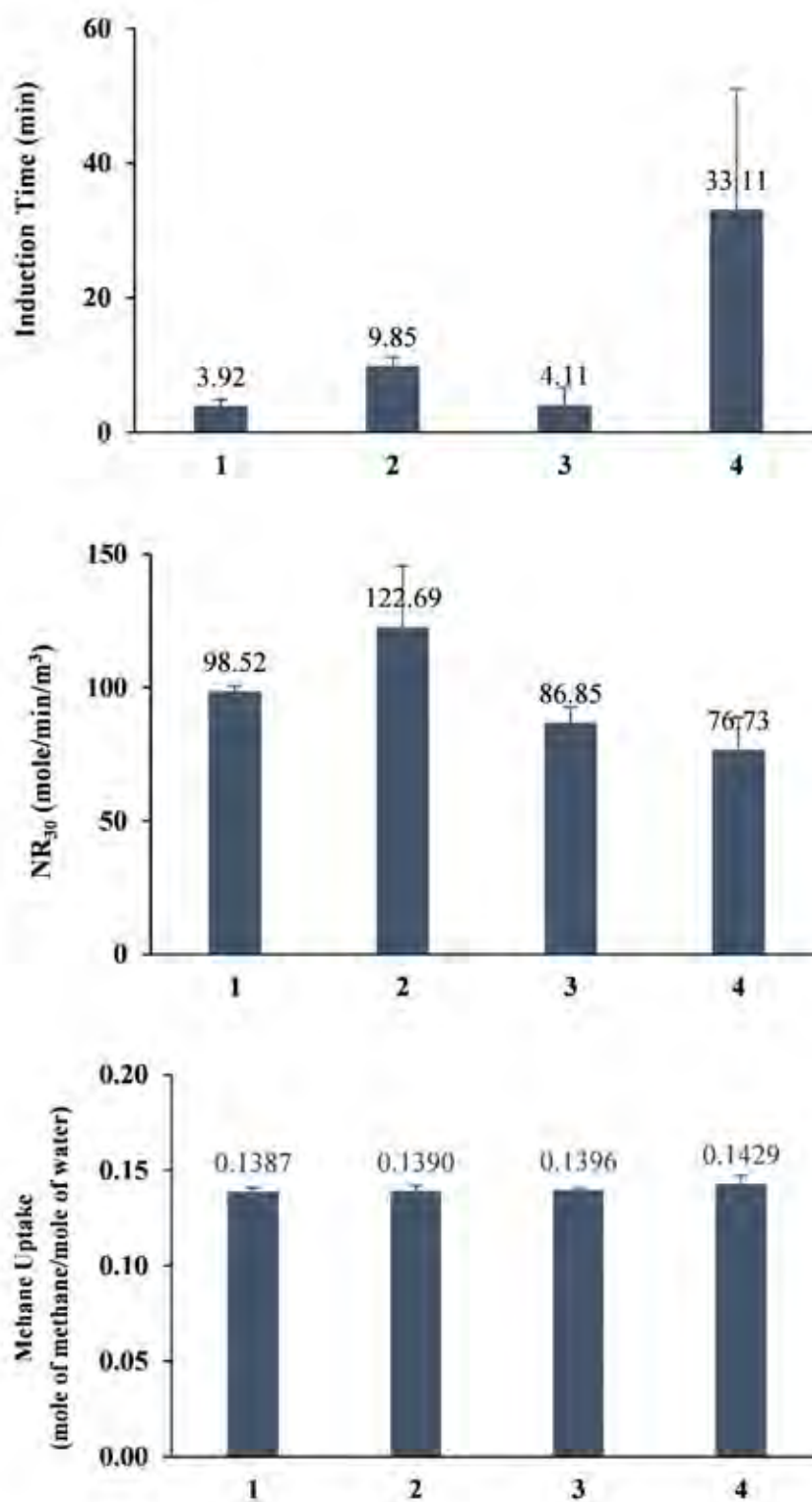
Figure 4.27 Comparison of methane hydrate formation kinetics in the presence of (1) 0.25 wt% SDS; (2) 0.25/0.25 wt% EO_3/SDS; (3) 0.25/0.25 wt% EO_5/SDS; (4) 0.25/0.25 wt% APG/SDS at 8 MPa and 4 °C in the quiescent condition.

CHAPTER 5
CONCLUSIONS

5.1 Conclusions

This work was carried out to study the effects of mixed SDS with nonionic surfactants, including EO_3, EO_5, and APG, on the methane hydrate kinetics, morphology, and foam suppression. The experiment was conducted at 8 MPa, 4 °C, and three different mass fractions, 0.25/0.0625 wt%, 0.25/0.125 wt%, and 0.25/0.25 wt% nonionic surfactant/SDS in the quiescent condition. The result showed that, in the presence of 0.25 wt% SDS, the induction time was 3.92 min, NR_{30} was 100.00 mol/min/m^3, and the methane uptake was 0.1402 mol of methane/mol of water. The additional of 0.0625 wt%, 0.125 wt%, and 0.25 wt% EO_3 resulted in the gradual increase in the induction time with the addition of higher concentration of EO_3, while there was no significant difference for the NR_{30} and methane uptake. Adding 0.0625 wt%, 0.125 wt%, and 0.25 wt% EO_5 showed the stochastic phenomenon on the induction time and NR_{30}, while the methane uptake was no different. The presence of 0.0625 wt%, 0.125 wt%, and 0.25 wt% APG increased the induction time 3, 5, and 10 times, respectively, compared to only 0.25 wt% SDS. The increase in the APG concentration resulted in the low rate of hydrate formation except for 0.0625 wt% APG, while the methane uptake was no different. Furthermore, an average yield of 79.57-86.84% was achieved on methane hydrate formation for every condition. Moreover, the morphology of hydrate formation and hydrate dissociation showed the similar pattern for all experiments. Interestingly, EO_3 reduced the foam generation during the hydrate dissociation with every concentration of EO_3, while the addition of 0.0625 wt% and 0.125 wt% EO_5 did not reduce the foam formation but 0.25 wt% EO_5 showed the optimum foam reduction compared to other conditions. Finally, adding 0.25/0.25 wt% APG/SDS lowered the foam formation during hydrate dissociation similar to 0.25/0.25 wt% EO_5/SDS but 0.0625 wt% and 0.125 wt% did not.

5.2 Recommendations

In order to suppress the amount of foam formation from using SDS as a kinetic promoter, another type of defoamer should be selected to get the effective foam reduction and not affecting the methane hydrate kinetics. Gemini surfactants are one of them, which could be mixed with SDS to eliminate the foam generation.

APPENDICES

Appendix A Calculation

- Methane gas consumption

From; $\quad \Delta n_{H,\downarrow} = n_{H,0} - n_{H,t} = \left(\dfrac{PV}{zRT}\right)_{G,0} - \left(\dfrac{PV}{zRT}\right)_{G,t}$

Where $\quad \Delta n_{H,\downarrow}$ = moles of consumed gas for hydrate formation, (mole)

$n_{H,0}$ = moles of hydrate at time 0, (mole)

$n_{H,t}$ = moles of hydrate at time t, (mole)

P = pressure in the system, (atm)

T = temperature in the system, (K)

V = volume of gas phase in the crystallizer, (cm^3)

Z = compressibility factor Pitzer's correlation

R = the universal gas constant 82.06 cm^3.atm/mol.K

- Methane gas uptake

From; $\quad$ Methane gas uptake $= \dfrac{(\Delta n_{H,\downarrow})_t}{n_{H_2O}}$

Where $\quad \Delta n_{H,\downarrow}$ = moles of consumed gas for hydrate formation, (mole)

n_{H_2O} = number of moles of hydrate at the start of the experiment

- Rate of hydrate formation

From; $$NR_t = \frac{R_t}{V_{water}}$$

Where R_t = the rate of hydrate growth (mmol/min)

V_{water} = volume of water taken in the reactor (m^3)

- Moles of methane gas release

From; $$\Delta n_{H,\uparrow} = n_{H,t} - n_{H,0} = \left(\frac{PV}{zRT}\right)_{G,t} - \left(\frac{PV}{zRT}\right)_{G,0}$$

- Methane recovery

From; $$\%methane\ recovery = \frac{(\Delta n_{H,\uparrow})}{(\Delta n_{H,\downarrow})} \times 100$$

Where $\Delta n_{H,\uparrow}$ = moles of released gas from hydrate during the hydrate dissociation at any given time.

$(\Delta n_{H,\downarrow})_{End}$ = moles of gas consumption for hydrate formation at the end of experiments.

- Hydrate yield

From; $$\%hydrate\ yield = \frac{\Delta n_{H,\downarrow}\ x\ Hydration\ number}{n_{H_2O}} \times 100$$

Where Hydration number = number of water molecules require per gas molecule to form the hydrate structures.

Properties of additive

Density of sodium dodecyl sulfate (SDS)	=	1.01	g/cm^3
Density of polyoxyethylene (3) lauryl ether (EO$_3$)	=	0.936	g/cm^3
Density of of polyoxyethylene (5) lauryl ether (EO$_5$)	=	0.941	g/cm^3
Density of alkyl poly glycol (APG)	=	0.934	g/cm^3

Appendix B Supporting information

Figure B1 Investigation on foam formation in the presence of nonionic surfactants at room temperature and 1 atm.

REFERENCES

Babu, P., Kumar, R., and Linga, P. (2013). Pre-combustion capture of carbon dioxide in a fixed bed reactor using the clathrate hydrate process. Energy, 50, 364-373.

Babu, P., Linga, P., Kumar, R., and Englezos, P. (2015). A review of the hydrate based gas separation (HBGS) process for carbon dioxide pre-combustion capture. Energy, 85, 261-279.

Bhattacharjee, G., Barmecha, V., Kushwaha, O. S., and Kumar, R. (2018). Kinetic promotion of methane hydrate formation by combining anionic and silicone surfactants: Scalability promise of methane storage due to prevention of foam formation. The Journal of Chemical Thermodynamics, 117, 248-255.

Bhattacharjee, G., Barmecha, V., Pradhan, D., Naik. R., Zare, K., Mawlankar, R., Dastager, S., Kushwaha, O., and Kumar, R. (2017). The biosurfactant Surfactin as a kinetic promoter for methane hydrate formation. Energy Procedia, 105, 5011-5017.

Bhattacharjee, G., Veluswamy, H., Kumar, R., and Linga, P. (2020). Seawater based mixed methane-THF hydrate formation at ambient temperature conditions. Energy, 271, 115-158.

Chaisalee, R., Soontravanich, S., Yanumet, N., and Scamehorn, J. (2003). Mechanism of Antifoam Behavior of Solutions of Nonionic Surfactants Above the Cloud Point. Surfactants and Detergents, 6, 345-351.

Gabitto, J. F., and Tsouris, C. (2010). Physical Properties of Gas Hydrates: A Review. Journal of Thermodynamics, 2010, 1-12.

Ganji, H., Manteghian, M., Zadeh, K., Omidkhanh, M., and Mofrad, H. (2007b). Effect of different surfactants on methane hydrate formation rate, stability and storage capacity. Fuel, 86, 434-411.

Hao, W., Wang, J., Fan, S., and Hao, W. (2008). Evaluation and analysis method for natural gas hydrate storage and transportation processes. Energy Conversion and Management, 49(10), 2546-2553.

Inkong, K., Veluswamy, H., Rangsunvigit, P., Kulprathipanja, S., and Linga, P. (2019). Investigation on the kinetics of methane hydrate formation in the presence of methyl ester sulfonate. Natural Gas Science and Engineering, 71, 102999.

of methane from hydrate formed in a variable volume bed of silica sand particles. Energy & Fuels, 23(11), 5508-5516.

Lozano-Castelló, D., Alcañiz-Monge, J., de la Casa-Lillo, M. A., Cazorla-Amorós, D., and Linares-Solano, A. (2002). Advances in the study of methane storage in porous carbonaceous materials. Fuel, 81(14), 1777-1803.

Jones, C., Dourado, J., and Chaves, H. (2010). Gas Hydrate and Microbiological Processes. Geoscience, 8, 0081.

Kalogerakis, N., Jamaluddin, A., Dholabhai, P., and Bishnoi, P. (1993). Effect of Surfactants on Hydrate Formation Kinetics. Society of Petroleum Engineers, 2, 51-88.

Kang, D. H., Yun, T. S., Kim, K. Y., and Jang, J. (2016). Effect of hydrate nucleation mechanisms and capillarity on permeability reduction in granular media. Geophysical Research Letters, 43(17), 9018-9025.

Khurana, M., Yin, Z., and Linga, P. (2017). A review of clathrate hydrate nucleation. ACS Sustainable Chemistry & Engineering, 5(12), 11176-11203.

Koh, C. A., Sloan, E. D., Sum, A. K., and Wu, D. T. (2011). Fundamentals and applications of gas hydrates. Chemical Biomolecular Engineering, 2, 237-257.

Kumar, A., Bhattacharjee, G., Kulkarni, B. D., and Kumar, R. (2015). Role of Surfactants in Promoting Gas Hydrate Formation. Industrial & Engineering Chemistry Research, 54(49), 12217-12232.

Kumar, A., Veluswamy, H. P., Linga, P., and Kumar, R. (2019). Molecular level investigations and stability analysis of mixed methane-tetrahydrofuran hydrates: Implications to energy storage. Fuel, 236, 1505-1511.

Levitz, P. (2002). Non-ionic surfactants adsorption: structure andthermodynamics. Geoscience, 334, 665-673.

Lin, W., Chen, G. J., Sun, C. Y., Guo, X. Q., Wu, Z. K., Liang, M. Y., Chen, L. T., and Yang, L. Y. (2004). Effect of surfactant on the formation and dissociation kinetic behavior of methane hydrate. Chemical Engineering Science, 59(21), 4449-4455.

Linga, P., Haligva, C., Nam, S. C., Ripmeester, J. A., and Englezos, P. (2009). Recovery

of methane from hydrate formed in a variable volume bed of silica sand particles. Energy & Fuels, 23(11), 5508-5516.

Lozano-Castelló, D., Alcañiz-Monge, J., de la Casa-Lillo, M. A., Cazorla-Amorós, D., and Linares-Solano, A. (2002). Advances in the study of methane storage in porous carbonaceous materials. Fuel, 81(14), 1777-1803.

McClure, D. D., Lamy, M., Black, L., Kavanagh, J. M., and Barton, G. W. (2017). An experimental investigation into the behaviour of antifoaming agents. Chemical Engineering Science, 160, 269-274.

Nakama, Y. (2017). Surfactants. *Cosmetic Science and Technology* (pp. 231-244).

Pandey, G., Bhattacharjee, G., Veluswamy, H. P., Kumar, R., Sangwai, J. S., and Linga, P. (2018). Alleviation of Foam Formation in a Surfactant Driven Gas Hydrate System: Insights via a Detailed Morphological Study. ACS Applied Energy Materials, 1(12), 6899-6911.

Posteraro, D., Pasieka, J., Maric, M., and Servio, P. (2016). The effect of hydrate promoter SDS on methane dissolution rates at the three phase (H-Lw-V) equilibrium condition. Journal of Natural Gas Science and Engineering, 35, 1579-1586.

Rhein, L. (2007). *Surfactant Action on Skin and Hair: Cleansing and Skin Reactivity Mechanisms* (I. Johansson and P. Somasundaran Eds.). Fairleigh Dickinson University, Teaneck, NJ, USA.

Sapag, K., Vallone, A., Blanco, A. G., and Solar, C. (2010). Adsorption of Methane in Porous Materials as the Basis for the Storage of Natural Gas. In P. Potocnik (Ed.), *Natural Gas* (pp. 205-244). New York: IntechOpen.

Siangsai, A., Rangsunvigit, P., Kitiyanan, B., Kulprathipanja, S., and Linga, P. (2015). Investigation on the roles of activated carbon particle sizes on methane hydrate formation and dissociation. Chemical Engineering Science, 126, 383-389.

Sloan. (2003). Fundamental principles and applications of natural gas hydrates. Nature, 426, 353-359.

Sloan, E. D., and Koh, C. A. (2008). *Clathrate Hydrates of Natural Gases*. New York:

CRC Press.

Smith, J. M., Van Ness, H. C., and Abbott, M. M. (2005). *Introduction to Chemical Engineering Thermodynamics*. Singapore: McGraw-Hill.

Som, I., Bhatia, K., and Yasir, M. (2011). Status of surfactants as penetration enhancers in transdermal drug delivery. Pharmacy and Bioallied Sciences, 4(1), 2-9.

Speight, J. (2008). *Natural gas. A Basic Hand Book*: Gulf Publishing Company.

Sum, A., Burruss, R., and Sloan, E. (1997). Measurement of Clathrate Hydrates via Raman Spectroscopy. American Chemical Society, 101, 7371-7377.

Sun, J., Brady, T. A., Rood, M. J., Lehmann, C. M., Rostam-Abadi, M., and Lizzio, A. A. (1997). Adsorbed Natural Gas Storage with Activated Carbons Made from Illinois Coals and Scrap Tires. Energy & Fuels, 11(2), 316-322.

Veluswamy, H. P., Ang, W. J., Zhao, D., and Linga, P. (2015). Influence of cationic and non-ionic surfactants on the kinetics of mixed hydrogen/tetrahydrofuran hydrates. Chemical Engineering Science, 132, 186-199.

Veluswamy, H. P., Hong, Q. W., and Linga, P. (2016a). Morphology study of methane hydrate formation and dissociation in the presence of amino acid. Crystal Growth & Design, 16(10), 5932-5945.

Veluswamy, H. P., Kumar, A., Kumar, R., and Linga, P. (2017). An innovative approach to enhance methane hydrate formation kinetics with leucine for energy storage application. Applied Energy, 188, 190-199.

Veluswamy, H. P., Kumar, A., Seo, Y., Lee, J. D., and Linga, P. (2018). A review of solidified natural gas (SNG) technology for gas storage via clathrate hydrates. Applied Energy, 216, 262-285.

Veluswamy, H. P., Kumar, S., Kumar, R., Rangsunvigit, P., and Linga, P. (2016b). Enhanced clathrate hydrate formation kinetics at near ambient temperatures and moderate pressures: Application to natural gas storage. Fuel, 182, 907-919.

Veluswamy, H. P., Prasad, P. S. R., and Linga, P. (2016c). Mechanism of methane hydrate formation in the presence of hollow silica. Korean Journal of Chemical Engineering, 33(7), 2050-2062.

Yin, Z., and Linga, P. (2019). Methane hydrates: A future clean energy resource. Chinese Journal of Chemical Engineering, 27(9), 2026-2036.

Yoslim, J., Linga, P., and Englezos, P. (2010). Enhanced growth of methane-propane clathrate hydrate crystals with sodium dodecyl sulfate, sodium tetradecyl sulfate, and sodium hexadecyl sulfate surfactants. Crystal Growth, 313, 68-80.

Zhang, J., Lee, S., and Lee, J. (2007). Kinetics of Methane Hydrate Formation from SDS Solution. American Chemical Society, 46, 6353-6359.

Zhu, X., Wang, D., and Craig, V. S. J. (2019). Interaction of Particles with Surfactant Thin Films: Implications for Dust Suppression. Langmuir, 35, 7641-7649.

Discover. (2014). In a world first, Japan extracted natural gas from frozen undersea deposits this year. https://www.discovermagazine.com/environment/japan-extracts-methane-from-fire-ice

EIA. (2018). Natural Gas - Energy Explained. from U.S. Energy Information Administration. Retrieved from https://www.eia.gov/energyexplained/natural-gas/

Oxiteno. (2018). Alcohol Ethoxylates. https://www.oxiteno.us/what-is-alcohol-ethoxylate-uses/

Wikiwand. (2018). Hydrophilic-lipophilic balance. https://www.wikiwand.com /en/ Hydrophilic-lipophilic_balance.

VITA

NAME   Chakorn Viriyakul

DATE OF BIRTH   13 Sep 1995

PLACE OF BIRTH   Singburi

INSTITUTIONS   Faculty of Engineering and Industrial Technology
ATTENDED   Silpakorn University
HOME ADDRESS   249 Village No.16 Sub-district. Boong District.
                                Muengamnatcharoen Amnatchareon Province 37000